

Visualizing Dependence in High-Dimensional Data: An Application to S&P 500 Constituent Data

Marius Hofert¹, Wayne Oldford²

2022-01-24

Abstract

The notion of a zenpath and a zenplot is introduced to search and detect dependence in high-dimensional data for model building and statistical inference. By using any measure of dependence between two random variables (such as correlation, Spearman's rho, Kendall's tau, tail dependence etc.), a zenpath can construct paths through pairs of variables in different ways, which can then be laid out and displayed by a zenplot. The approach is illustrated by investigating tail dependence and model fit in constituent data of the S&P 500 during the financial crisis of 2007–2008. The corresponding Global Industry Classification Standard (GICS) sector information is also addressed.

Zenpaths and zenplots are useful tools for exploring dependence in high-dimensional data, for example, from the realm of finance, insurance and quantitative risk management. All presented algorithms are implemented using the R package `zenplots` and all examples and graphics in the paper can be reproduced using the accompanying demo `SP500`.

Keywords

Zenpath, zenplot, detecting dependence, high dimensions, graphical tools.

MSC2010

62-09, 62H99, 65C60

1 Introduction

Motivated by the use of high-dimensional data such as data from several hundred risk-factor changes in the realm of quantitative risk management, we raise the following simple question:

How can one detect and visualize dependence in high-dimensional data?

¹Department of Statistics and Actuarial Science, University of Waterloo, 200 University Avenue West, Waterloo, ON, N2L 3G1, marius.hofert@uwaterloo.ca. The author would like to thank NSERC for financial support for this work through Discovery Grant RGPIN-5010-2015.

²Department of Statistics and Actuarial Science, University of Waterloo, 200 University Avenue West, Waterloo, ON, N2L 3G1, rwoldford@uwaterloo.ca.

Detecting and visualizing dependence in high-dimensional data is important for model building and inference in areas such as finance, insurance and quantitative risk management, where the one-period ahead behaviour of a high-dimensional portfolio represented by a random vector $\mathbf{X} = (X_1, \dots, X_d)$, d large, is studied; see McNeil et al. (2015, Section 2.2.1).

The example we consider in this work is that of detecting and visualizing tail dependence of a portfolio consisting of sign-adjusted log-returns of all constituents of the S&P 500, so we have realizations $(X_{t,j})_t$ of $X_j = X_{t,j} = -\log(S_{t,j}/S_{t-1,j})$, $j \in \{1, \dots, d\}$, for $d \approx 500$, and $S_{t,j}$ denotes the end-day price of constituent j of the S&P 500 at time $t \in \{1, \dots, T\}$. To each component of this high-dimensional data, we fit an ARMA(1, 1) – GARCH(1, 1) model, extract the corresponding standardized residuals and (for illustration) investigate their tail dependence in the so-called *copula-GARCH* framework (see Patton (2006) and Patton (2013)) by considering the pseudo-observations of the standardized residuals. We also address graphical assessment of model fit.

The high dimensions we consider in this paper are of the order of hundreds. Dimensionality reduction is often not a practical option when, for example, components X_j , $j \in \{1, \dots, d\}$, are each individually of interest and need to be tracked (such as for portfolios of life insurance contracts). Computationally, this is already fairly demanding, requiring, for example, efficient algorithms to estimate a (Student) t copula in large dimensions. Providing meaningful displays of such high dimensional output adds to this challenge.

Our running example will be the S&P 500 constituent data. The source, the time-series models we fit, and the connection with copulas, are all described in Section 2. This setup provides the high-dimensional model output that will then be visualized. Section 3 presents the zenplot, a compact graphical presentation of high-dimensional data arranged in a path of one- and two-dimensional displays. When dimensions are high it will often be necessary to draw attention to, and to display, only the most salient features of the data. To this end, Section 3.2 introduces the notion of a zenpath, a tool to provide an interesting path through the pairs of variables. In Section 4, zenpaths are then applied in the context of model assessment and model comparison. Different measures are used to illustrate a variety of zenplots that naturally arise in model criticism and selection whenever the number of dimensions becomes large. All graphs in this paper can be reproduced with the demo SP500 provided in the R package `zenplots`; see Hofert and Oldford (2016). In the last section we provide concluding remarks.

2 S&P 500 constituent data

We consider time series of all 505 constituents of the S&P 500 as of 2015-10-12; see https://en.wikipedia.org/wiki/List_of_S%26P_500_companies and note that the S&P 500 does not necessarily have exactly 500 constituents. However, our interest lies in the 756 trading days between 2007-01-01 ($t = 0$) and 2009-12-31 ($t = T$) which contains the global financial crisis of 2007–2008. This data was downloaded from a publicly available source (<https://finance.yahoo.com/> on 2016-01-03) and then incorporated into the R package

2 S&P 500 constituent data

`qrmdata`; see Hofert and Hornik (2016). We assume that the order of the data is according to their Global Industry Classification Standard (GICS) information (see the demo `SP500` of the R package `zenplots`). Of course any company joining the S&P 500 after 2009-12-31 will not appear in this period and, for the remainder there can be much data missing.

To assess the extent of the missing data, we plot in Figure 1 (left-hand side) the days

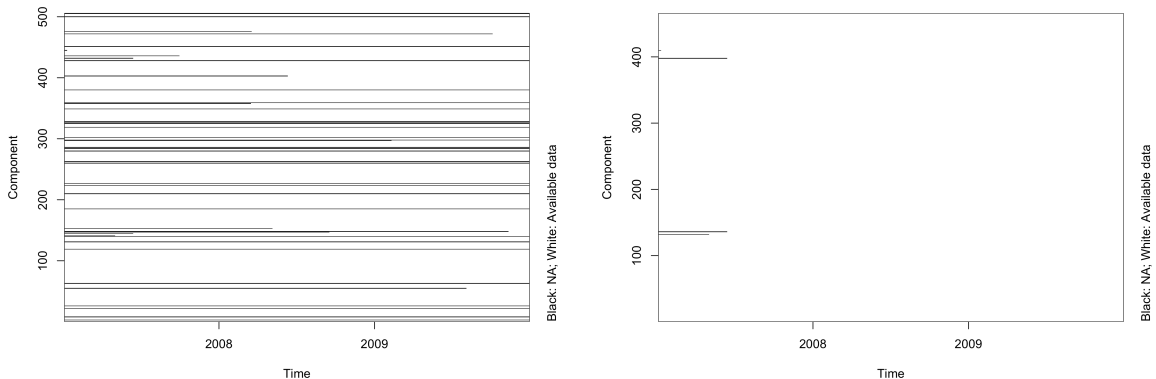


Figure 1 Missing data for all 505 S&P 500 constituents from 2007-01-01 to 2009-12-31 (left-hand side); days with missing data are marked for each constituent. We work with the 465 constituents with maximally 20% missing data (right-hand side) and fill the missing data via `na.fill(, fill = "extend")`.

missing a value for each of the 505 constituents. The missing data pattern likely indicates that many of the constituents joined the S&P 500 in this period (or after for those whose lines span the time period). We are still left with 465 companies if we retain only those having at least 80% complete data. As the right-hand side of Figure 1 shows, only four of these have any data missing (those are `DAL` (Delta Air Lines), `DFS` (Discover Financial Services), `TEL` (TE Connectivity Ltd.) and `TWC` (Time Warner Cable)). We restrict our analysis to these 465 constituents and fill the missing data of the four components with R's `na.fill(, fill = "extend")`. This function interpolates linearly between adjacent data where available and, otherwise, repeats the leftmost or rightmost available data. In the end, we will work with a complete data set having $T = 756$ daily records on $d = 465$ dimensions.

2.1 Modelling the margins

We will first model the 755 negative log-returns for each of the 465 constituents. Given our time horizon and the financial crisis of 2007–2008, we cannot assume each constituent series of negative log-returns to be realizations of independent and identically distributed (iid) random variables. Instead, we need to incorporate some serial (temporal) dependence for each series. Because of the large number of marginal time series, we take a broad-brush approach and use the popular `ARMA(1, 1)`–`GARCH(1, 1)` model for each margin separately (a process also known as `de-GARCHing`).

These models have the form

$$\begin{aligned} X_{t,j} &= \mu_{t,j} + \varepsilon_{t,j} \quad \text{for} \quad \varepsilon_{t,j} = \sigma_{t,j} Z_{t,j}, \\ \mu_{t,j} &= \mu_j + \phi_j(X_{t-1,j} - \mu_j) + \theta_j(X_{t-1,j} - \mu_{t-1,j}), \\ \sigma_{t,j}^2 &= \alpha_{j0} + \alpha_{j1}(X_{t-1,j} - \mu_{t-1,j})^2 + \beta_j \sigma_{t-1,j}^2, \end{aligned}$$

where, for all components $j \in \{1, \dots, d\}$, $\mu_j \in \mathbb{R}$, $|\phi_j| < 1$, $|\theta_j| < 1$, $\alpha_{j0} > 0$, $\alpha_{j1} \geq 0$, $\beta_j \geq 0$, $\alpha_{j1} + \beta_{jk} < 1$.

The stochastic component $Z_{t,j}$ for each series $j \in \{1, \dots, d\}$ are the *innovations*; their empirical counterparts on which our analysis is based later on are known as *standardized residuals*. For each series the innovations are taken to be iid, centred about zero and having unit variance. We model the innovation distribution as a scaled (Student) t distribution; that is, for each $j \in \{1, \dots, d\}$, $Z_{t,j} \stackrel{\text{iid.}}{\sim} F_j(z) = t_{\nu_j}(z\sqrt{\nu_j/(\nu_j - 2)})$, where t_{ν_j} is the distribution function of the standard t distribution with ν_j degrees of freedom.

Even though each series is fit separately, the fitting itself is non-trivial for so many components. We thus use the robust `fit_ARMA_GARCH()` from `qrmtools` (developed for this purpose; see Hofert and Hornik (2015)) with `solver = "hybrid"` for the underlying fitting procedure `ugarchfit()` of the R package `rugarch` of Ghalanos (2011). The six warnings which appear can safely be ignored here as they only indicate issues in finding initial values for the fitting; see the demo for more details. The estimated standardized residuals $\hat{\mathbf{Z}}_t = (\hat{Z}_{t,1}, \dots, \hat{Z}_{t,d})$, $t \in \{1, \dots, T\}$ from this fit will be treated as realizations of \mathbf{Z}_t in any subsequent analysis. Residual checks are presented in Section 4.2.

2.2 Modelling cross-sectional dependence

Having modelled the component series marginally, we turn our attention to the multivariate series of standardized residuals $(\mathbf{Z}_t)_t$ for iid $\mathbf{Z}_t = (Z_{t,1}, \dots, Z_{t,d}) \sim H$, where H has continuous margins F_j , $j \in \{1, \dots, d\}$, as described before. By Sklar's Theorem, see Sklar (1959), the joint distribution function H of \mathbf{Z}_t can be decomposed as

$$\begin{aligned} H(z_1, \dots, z_d) &= C(F_1(z_1), \dots, F_d(z_d)), \quad \mathbf{z} \in \mathbb{R}^d \\ &= C(u_1, \dots, u_d), \quad \mathbf{u} \in [0, 1]^d, \end{aligned}$$

for some copula C , where $u_j = F_j(z_j)$, $j \in \{1, \dots, d\}$. The copula C determines the dependence between $Z_{t,1}, \dots, Z_{t,d}$. Since $u_j = F_j(z_j)$, the copula is itself a distribution function having marginal $U(0, 1)$ distributions.

In practice, we do not observe data from C , but rather from H . So to estimate C we work with *pseudo-observations* constructed from the available standardized residuals $\hat{\mathbf{Z}}_t = (\hat{Z}_{t,1}, \dots, \hat{Z}_{t,d})$, $t \in \{1, \dots, T\}$. Based on the estimated margins \hat{F}_j of F_j , $j \in \{1, \dots, d\}$, the pseudo-observations of C are computed via $\hat{F}_j(\hat{Z}_{t,j})$, $t \in \{1, \dots, T\}$, $j \in \{1, \dots, d\}$. One could take the fitted scaled t distributions mentioned earlier as $\hat{F}_1, \dots, \hat{F}_d$. However, model misspecification could affect estimation of C , particularly for large dimensions.

3 Visualizing dependence in high dimensions with zenplots

Consequently, we prefer to work with the marginal empirical distribution functions $\hat{F}_{T,j}$ for $j \in \{1, \dots, d\}$ and their pseudo-observations

$$U_{t,j} = \frac{T}{T+1} \hat{F}_{T,j}(\hat{Z}_{t,j}) = \frac{R_{t,j}}{T+1} \quad (1)$$

where $R_{t,j}$ denotes the rank of $\hat{Z}_{t,j}$ among $\hat{Z}_{1,j}, \dots, \hat{Z}_{T,j}$ (the scaling factor $\frac{T}{T+1}$ avoids having any estimated value of a distribution function be exactly one). Moreover, Genest and Segers (2010) have shown that estimators based on these pseudo-observations can be asymptotically more efficient (even when the marginal distributions are known).

The observed joint distribution of the pseudo-observations can then be used to provide insight on the copula function C and hence the underlying stationary cross-sectional dependence.

3 Visualizing dependence in high dimensions with zenplots

A scatterplot of the pseudo-observations $U_{t,j}$, $t \in \{1, \dots, T\}$, $j \in \{1, \dots, d\}$ can reveal a lot of information about the dependence structure between any pair of variates and can give some sense of what features the underlying unknown copula model has. To simplify the demonstration of this based on our S&P 500 data, consider all columns (or components) sorted according to their GICS sectors in alphabetical order (together with the number of constituents of that sector): “Consumer discretionary” (78), “Consumer staples” (33), “Energy” (36), “Financials” (85), “Health care” (51), “Industrials” (63), “Information technology” (60), “Materials” (25), “Telecommunications services” (5), and “Utilities” (29). Within each sector, the original order of the components remains untouched. From left to right, Figure 2 shows a scatterplot of independent $U(0,1)^2$ observations followed by plots of

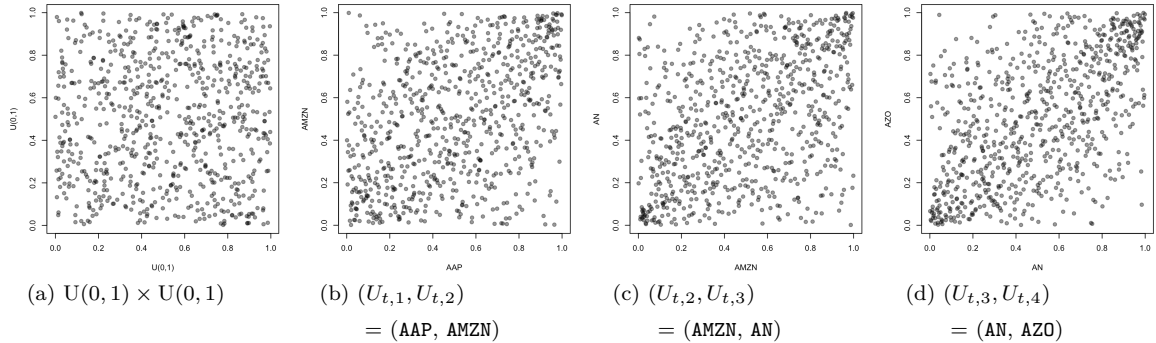


Figure 2 Scatterplots of (a) independent $U(0,1)$ random variables and (b, c, d) the pseudo-observation pairs $(U_{t,j}, U_{t,j+1})$, $j \in \{1, 2, 3\}$. Ticker symbol abbreviations: AAP = Advanced Auto Parts, AMZN = Amazon.com Inc., AN = AutoNation Inc., and AZO = AutoZone Inc.

the pseudo-observations for a few pairs of the S&P 500 constituents’ standardized residuals.

3 Visualizing dependence in high dimensions with zenplots

If the standardized residuals from a pair of stocks are statistically independent from one another, then this plot should be indistinguishable from points uniformly distributed over the unit square as, for example, they are in the left-most scatterplot of Figure 2.

Roughly speaking, the less the pseudo-observations look like independent uniforms the stronger is their dependence. For example, each of the three right-most plots in Figure 2 departs some from a uniform, though not dramatically. Each is a little sparser in the top left and bottom right corners and is a little denser in the bottom left and top right corners. Though somewhat weak, this shows a positive dependence between the standardized residuals of these pairs of stocks over this period in the sense that they tend to be jointly large or small. The strongest of the three appears to be the right-most plot in Figure 2 – as one might expect between the standardized residuals of AutoNation Inc. (AN) and AutoZone Inc. (AZO).

Figure 3 displays the scatterplot matrix of the pseudo-observations of the standardized residuals from marginally fitting the first 22 constituents of our S&P 500 data. In addition to being able to simultaneously display and compare many plots at once, the scatterplot matrix has another important characteristic when it comes to assessing dependence – it produces small scatterplots. Small scatterplots make our visual system focus on the low spatial frequency characteristics of each plot and this is ideal for detecting dependence structure from uniforms.

For example, consider again the plots of Figure 2. The right-most three plots appear in Figure 3 as the first three plots from the top left along the first diagonal above the main diagonal; that is, considering the scatterplot matrix as a 22×22 matrix, the right-most three plots of Figure 2 appear in cells (1, 2), (2, 3), and (3, 4), respectively, of the scatterplot matrix in Figure 3. Moving your eye along the first three plots of this diagonal, it is easier to see the dependence in each plot and that this dependence is increasing as the eye travels down and to the right. The same visual effect can be achieved with Figure 2 by squinting when observing the plots, or by physically moving farther away (and hence making them smaller).

Note that some care has been taken in the construction of the scatterplot matrix. No superfluous annotation appears (no axes, etc.), each point is plotted with a very small size, and the colour used for plotting includes an alpha level chosen so that overplotted points will show darker (so-called *alpha-blending*) to better visually suggest the density of the distribution.

Looking over the scatterplot matrix one can assess the (in)dependence of any pair and compare the strength of the dependence for different pairs. For example, considering only the top left 4×4 block, we can see that position (1, 4) shows the highest dependence in this block, with a preponderance of points in having high joint returns. This scatterplot is that of AZO and AAP and shows a stronger dependence than that of AZO and AN shown in (3, 4) or the right-most plot in Figure 2. In the rest of the matrix there are other stronger, and many weaker, types of dependence that can also be seen. The dependence that stands out most is that of CMCSA and CMCSK, near the diagonal in position (14, 15). These are the pseudo-observations for the standardized residuals on two different classes of Comcast

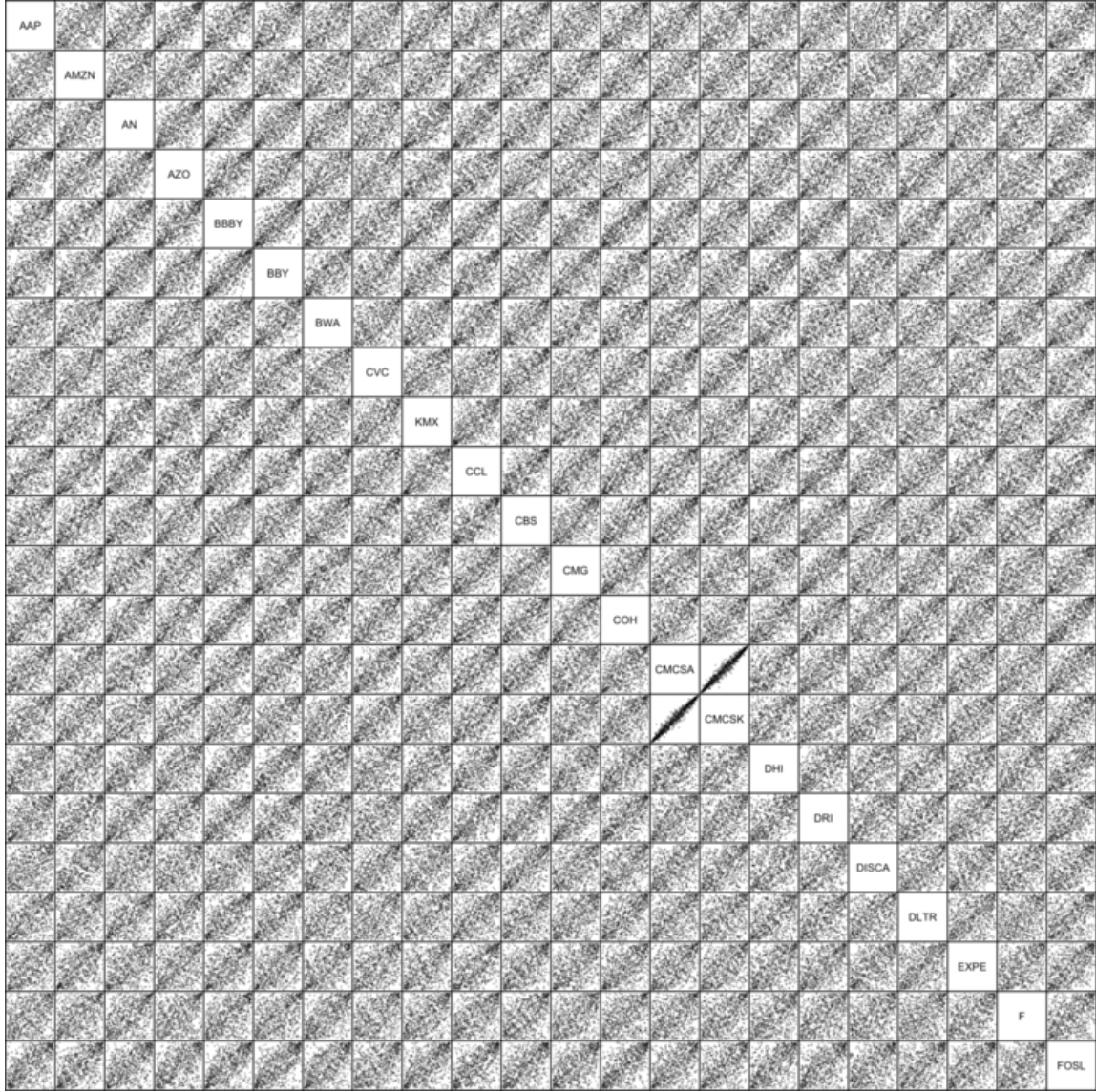


Figure 3 Scatterplot matrix of $(U_{t,j})_t, j \in \{1, \dots, 22\}$. Small displays highlight low spatial frequency structure, and hence dependence structure, and allow the dependence of many pairs to be assessed and compared simultaneously.

shares, which explains such a strong dependency.

3.1 Zenplots

A major drawback of the scatterplot matrix is its wasted space. Every plot appears twice, once above the main diagonal and once below – for example, the two strongest dependencies seen near the main diagonal of Figure 3 are the same pairs of Comcast constituents. In this display of 462 scatterplots, only 231 show different pairs (possibly after a rotation or reflection).

In contrast, a *zenplot* (or *zigzag expanded navigation plot*) lays out many more scatterplots by making better use of the space. The plots are laid out following a well defined path that zigzags across the page. Figure 4 shows a zenplot that displays $d - 1 = 464$ *different* scatterplots in approximately the same space; to this end we used the function `zenplot()` of the R package `zenplots`. As with the scatterplot matrix one sees two very strong dependencies. Unlike the scatterplot matrix, these are two different pairs of stocks: the one in the first row is that of the Comcast shares as before, but the one in the fourth row is a pair of two different classes of Twenty-first Century Fox shares (`FOX` and `FOXA`). The zenplot allows visual search and comparison over twice as many plots as does a scatterplot matrix in the same space; note that the labels of the pairs can be made more visible by zooming in on Figure 4.

The zenplot lays out the scatterplots as follows. The first is placed in the top left corner. This has variate 1 as its horizontal axis and variate 2 as its vertical. The next plot is placed at the right of the first with variate 2 as its vertical axis and variate 3 as its horizontal. The third scatterplot is placed below the second with variate 3 as its horizontal and variate 4 as its vertical. The next scatterplot is placed to the right of this sharing the same vertical axis and having variate 5 as its horizontal axis. Then the next plot is placed above the fourth with horizontal variate 5 and vertical variate 6. One zigzag pattern is now completed and we are in a position similar to the starting position. This continues left to right across the page until the end where the zigzag moves down and reverses its direction to move from right to left. And so on until all plots have been laid out. Whenever an axis is shared, the name of that variate appears between the two plots.

If one imagines the $d \times d$ scatterplot matrix of all d variates, the zenplot of Figure 4 has plotted all scatterplots that lie along the diagonal of the scatterplot matrix immediately above the main diagonal – it plots the pairs $(1, 2), (2, 3), \dots, (d-1, d)$. For example, the three scatterplots in the top left corner of Figure 4 are exactly the three right-most scatterplots of Figure 2. Many other customizations of zenplots are possible; see `?zenplot`.

3.2 Zenpaths

Although a zenplot shows twice as many distinct pairs as does a scatterplot matrix in the same space, there are still a great many pairs that could be shown. For $d = 465$ dimensions there are $\binom{d}{2} = 107,880$ distinct plots. Of these, the zenplot of Figure 4 showed a little

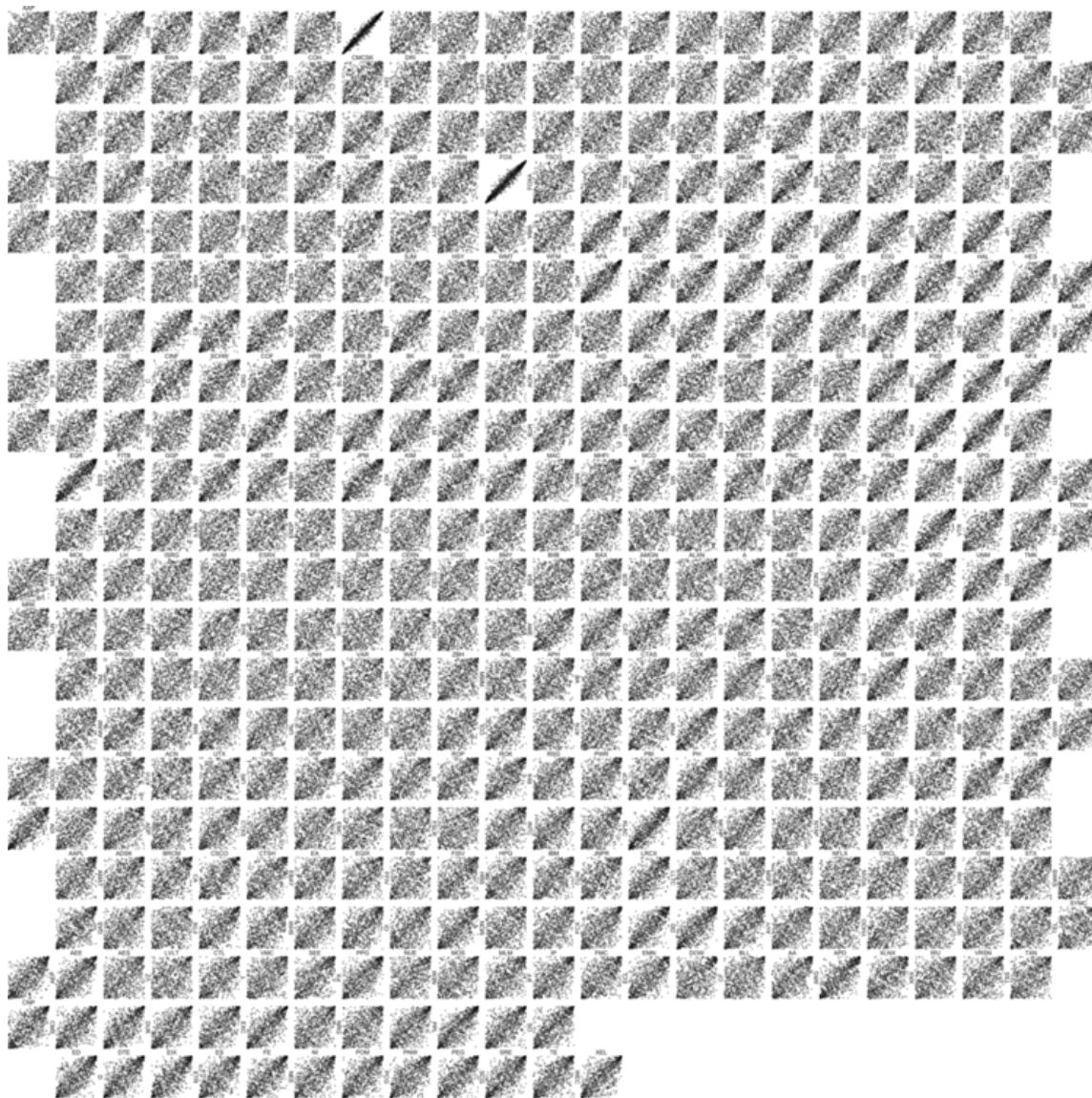


Figure 4 A zenplot of the pseudo-observations showing the pairs $(1, 2), (2, 3), \dots, (d - 1, d)$ for $d = 465$.

fewer than 500 or about 0.5% of all that are possible. To look at all plots would require more than 200 zenplots of the size of that shown in Figure 4 (or more than 400 scatterplot matrices); see also our comment in the last paragraph of Section 4 where we mention the exercise of laying out and actually examining all distinct pairs in a single zenplot.

Better would be to show only the *most interesting* pairs of plots. Here again the zenplot layout has an enormous advantage over the scatterplot matrix, simply by not being restricted to a matrix layout. Instead, the zenplot displays a particular path (or series of paths) through the scatterplot matrix.

To see this, imagine the $d \times d$ scatterplot matrix. A path can be followed through this matrix beginning at any plot and jumping to any other plot in the same row or column, thus sharing either a vertical or horizontal axis, and continuing in this fashion to produce a path of any desired length; see Hurley and Oldford (2011b). A *zenpath* is any such path which alternates between searching along a row and along a column (that is, it is a 3d transition path in the sense of Hurley and Oldford (2011b)).

A (default) zenplot display lays out the scatterplots in the order in which the variates appear in the dataset. Figure 4, for example, follows the variate order $1, \dots, d$ which corresponds to the zenpath starting at the top left corner of the scatterplot matrix of all d variates and zigzagging alternating right (same row) and downward (same column) crossing the variate name on the diagonal to the next plot each time. The path ends when the bottom right corner is reached. To follow any particular zenpath, then, the variate order in the dataset is simply changed to that of the desired zenpath before zenpath is called.

When a measure of interestingness can be assigned to each scatterplot, we might restrict our displays to show only those plots of high interest. These can be laid out as a zenpath (or series of disconnected zenpaths) following the graph theoretic methods of Hurley and Oldford (2010) and Hurley and Oldford (2011b) and automated using the R package *PairViz* of Hurley and Oldford (2011a).

For financial data like the S&P 500, interest often lies in the dependence between the negative log-returns of any two stocks. Two common dependence measures for such data are Kendall’s tau and Spearman’s rho (both are measures of concordance in the sense of Scarsini (1984)) on the standardized residuals. Or, as in certain quantitative risk management applications, we might be interested primarily in what happens in the extremes, that is in some measure of tail dependence between the two returns. In what follows, we focus on the latter case.

3.2.1 Tail dependence based on pairwise fitted t copulas

Here our measure of “interestingness” will be a formal measure of the (upper) tail dependence between each pair of negative log-returns by fitting bivariate copulas. To be concrete, for any (Z_1, Z_2) with joint distribution function H , continuous marginal distribution functions F_1, F_2 , and corresponding marginal quantile functions Q_1, Q_2 , a measure of upper tail dependence, for any $p \in [0, 1]$, can be taken to be $\mathbb{P}(Z_2 > Q_2(p) | Z_1 > Q_1(p))$. This probability is symmetric in Z_1 and Z_2 and the larger it is, the greater is the dependence

3 Visualizing dependence in high dimensions with zenplots

between Z_1 and Z_2 in the top right corner of the bivariate distribution. Taking its limit as $p \rightarrow 1$, we have the *coefficient of upper tail dependence*

$$\lambda = \lim_{p \uparrow 1} \mathbb{P}(Z_2 > Q_2(p) \mid Z_1 > Q_1(p)).$$

This is often of interest when modelling joint high quantile exceedances in quantitative risk management; see, for example, McNeil et al. (2015, Example 7.40). If the bivariate copula for H is C , then it is easy to show that

$$\lambda = \lim_{p \uparrow 1} \frac{1 - 2p + C(p, p)}{1 - p} \quad (2)$$

and so the coefficient depends only on the underlying copula C of H and not on the margins F_1, F_2 .

Although non-parametric estimation of λ is a possibility it requires deciding on how best to choose the number of data points $k = np$ or equivalently the probability level p on which to base estimation. For our purposes, it is enough to fit parametric copula models to the pseudo-observations (1) of each pair of variables and the implied tail-dependence coefficients be computed (based on equation (2)).

In higher dimensions practitioners have begun working with matrices $\Lambda = [\lambda_{ij}]$ of pairwise upper tail-dependence coefficients; see Embrechts et al. (2016) for a characterization and practical application. Estimates of the entries of Λ will be taken to be the pairwise estimates $\hat{\lambda}_{ij}$.

To this end we will use bivariate t copulas and fit them using the approach of Mashal and Zeevi (2002) (see also Demarta and McNeil (2005)) and the recently available implementation `fitCopula(, method = "itau.mpl")` from the R package `copula` of Hofert et al. (2017). In terms of the fitted degrees of freedom ν and the correlation ρ (the off-diagonal element of the bivariate t copula's scale matrix P), the upper tail-dependence coefficient λ of a t copula is

$$\lambda = 2t_{\nu+1} \left(-\sqrt{\frac{(\nu+1)(1-\rho)}{1+\rho}} \right), \quad (3)$$

where $t_{\nu+1}(x)$ is the distribution function of the t distribution on $\nu+1$ degrees of freedom evaluated at x . Replacing the parameters by their estimates gives an estimate for λ .

Figure 5 shows pairwise estimated upper tail-dependence coefficients λ for all $\binom{d}{2} = 107,880$ pairs. At left, these are displayed in a matrix arrangement analogous to a scatterplot matrix except that, instead of a scatterplot, in each cell the value of the corresponding λ estimate is shown using a grey-scale encoding of $[0, 1]$. This is essentially the pairwise estimated matrix Λ . At right, the overall density of all pairwise λ estimates is shown. Most values, for example, are less than 0.3.

The rows (columns) of the estimated matrix Λ are arranged in Figure 5 so that stocks in the same GICS sector, and within each sector in the same sub-sector, appear next to each

3 Visualizing dependence in high dimensions with zenplots

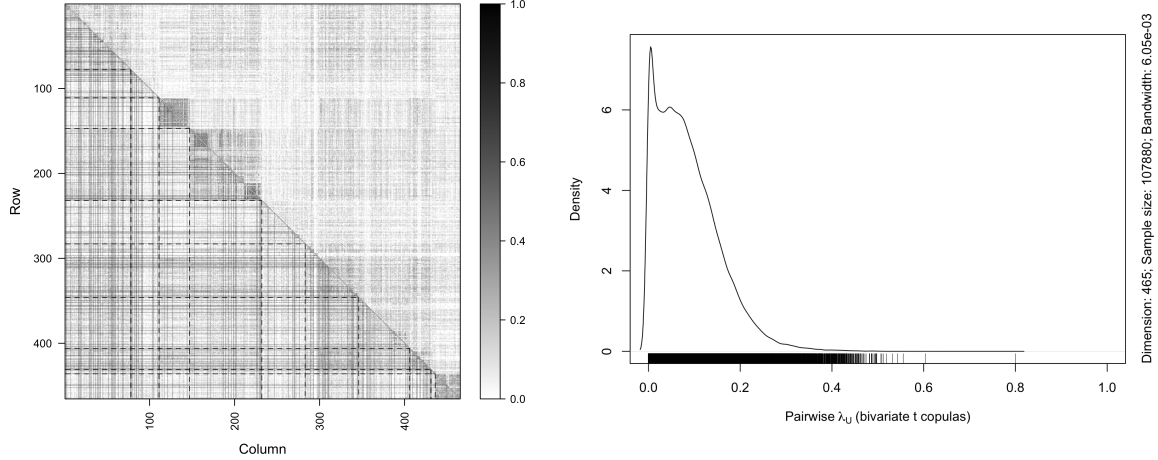


Figure 5 Pairwise estimated upper tail-dependence coefficients λ from fitted bivariate t copulas (different degrees of freedom). At left is the entire matrix Λ with GICS sectors (dashed lines) and sub-sectors (finer solid lines) indicated; at right is a plot of the estimated density of all $\binom{d}{2}$ pairwise entries of Λ .

other in the same row (column). The boundaries between sectors are marked by dashed lines appearing below the diagonal. The sectors appear top to bottom (left to right) in alphabetical order as before, namely: “Consumer discretionary” (78 constituents = first 78 rows), “Consumer staples” (33), “Energy” (36), “Financials” (85), “Health care” (51), “Industrials” (63), “Information technology” (60), “Materials” (25), “Telecommunications services” (5), and “Utilities” (29). Fine lines below the diagonal mark the sub-sectors within each sector (more easily discerned by zooming in on the display).

Even with such low estimated values for the upper tail-dependence coefficients, some structure is revealed by the estimated matrix Λ of Figure 5. The darkest blocks along the diagonal correspond to stocks in the same sector and within the same sub-sector. The third diagonal block down, for example, shows relatively stronger tail dependencies existing between constituents of the “Energy” sector. Such information can, for example, be used to set up a hierarchical dependence model with within-sector dependencies modelled differently than might be any between-sector dependencies. Off the diagonal, the very light region immediately above the dark diagonal “Energy” block suggests overall little dependence between the constituents of the “Energy” sector and those of the “Consumer staples” sector. The cell values of Λ can thus help determine which corresponding scatterplots of pseudo-observations to examine more closely along some zenpath(s) of interest.

Finding interesting zenpaths from Λ has been automated by the function `zenpath()`. In Figure 6 `zenpath()` was used to find the ten pairs having strongest upper tail dependence and the ten pairs having weakest upper tail dependence. All twenty plots are arranged in order from highest upper tail dependence to lowest upper tail dependence. The zigzag pattern is followed exactly as in Figure 4 except now there are occasional places showing

3 Visualizing dependence in high dimensions with zenplots

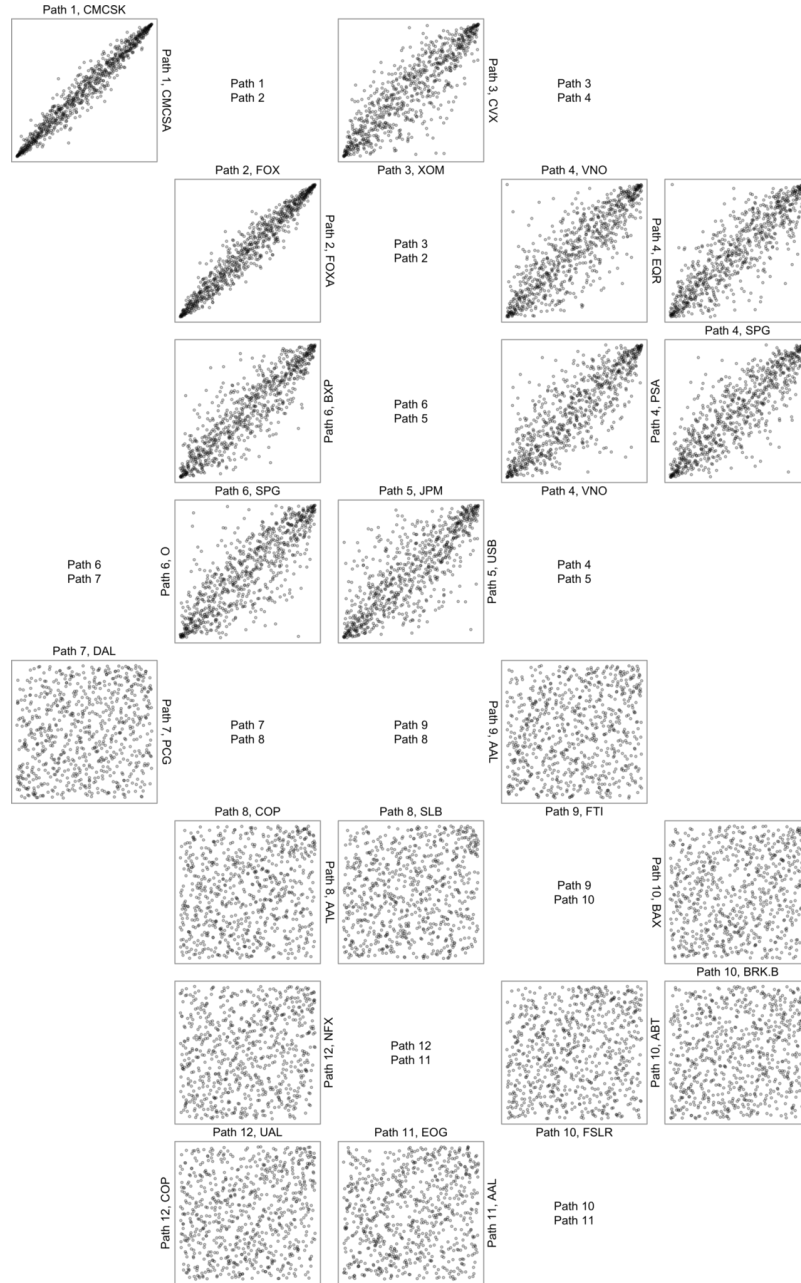


Figure 6 A zenplot constructed from a zenpath displaying the pseudo-observations of those 10 pairs of variables with largest (first) and then those 10 pairs with smallest (last) upper tail-dependence coefficient. When variables along the path are connected, they are displayed in one contiguous zenpath, abbreviated by Path 1–Path 12. Concatenated paths are separated by a block marking the transition from one path to another.

only a couple of labels where a scatterplot might have been expected. The reason for this is that these places mark boundaries where one zenpath ends and another one begins. Recall that a zenpath connects plots which share a variate (by alternating row and column selections in a scatterplot matrix). When no such variate is shared the zenpath ends and a new one begins (the change being equivalent to moving from one cell in a scatterplot matrix to another in a different row *and* different column). The zenplot of Figure 6 is the concatenation of twelve different zenpaths.

The two strongest upper tail-dependencies are those we have already seen, namely the two classes of Comcast shares and the two classes of Twenty-first Century Fox shares. Because these two pairs share no variates, they define the first two zenpaths (each of length one plot, or two variates) and are separated by the space labelling the end of path 1 and the beginning of path 2. The third path, also of length one, consists of the pair of stocks from the “Energy” sector, *CVX* (Chevron Corp.) and *XOM* (Exxon Mobil Corp.). Next is a path of length four, consisting of the variates *VNO* (Vornado Realty Trust), *EQR* (Equity Residential), *SPG* (Simon Property Group Inc), and *PSA* (Public Storage), all from the “Financials” sector. The stock *VNO* appears in two of these four pairs. Path 5 consists of the two “Financials” sector stocks *USB* (U.S. Bancorp) and *JPM* (JPMorgan Chase & Co.) and path 6 of three more, *BP* (Boston Properties), *SPG* (Simon Property Group Inc), and *O* (Realty Income Corporation). Note that every pair of variates, of the ten having the strongest upper tail-dependence coefficient, is formed from stocks from the same GICS sector and no variate turns up paired with another from a different sector.

The variate pairs with weakest upper tail dependence appear in the bottom half of Figure 6 and are essentially indistinguishable from uniform scatterplots (see Figure 2(a)). This suggests that these pairs of standardized residuals can be considered to be independent. There are again six paths: path 7 *DAL* (Delta Air Lines) from the “Industrials” sector, *PCG* (PG&E Corp.) from the “Utilities”, path 8 *COP* (ConocoPhillips) “Energy”, *AAL* (American Airlines Group) “Industrials”, and *SLB* (Schlumberger Ltd.) “Energy”, path 9 *AAL* (American Airlines Group) “Industrials”, and *FTI* (FMC Technologies Inc.) “Energy”, path 10 *BAX* (Baxter International Inc.) “Health Care”, *BRK.B* (Berkshire Hathaway) “Financials”, *ABT* (Abbott Laboratories) “Health Care”, and *FSLR* (First Solar Inc) “Information Technology”, path 11 *AAL* (American Airlines Group) “Industrials”, and *EOG* (EOG Resources) “Energy”, and finally path 12 *NFX* (Newfield Exploration Co) “Energy”, *UAL* (United Continental Holdings) “Industrials”, and *COP* (ConocoPhillips) “Energy”. Note that the ten pairs of variates with weakest upper tail dependence are from different GICS sectors.

Given that the weakest dependencies occur between constituents from different GICS sectors, one might ask what pairs of constituents from different sectors have the strongest upper tail dependencies. To answer this, Figure 7 shows the ten such cross sector pairs having greatest tail dependence in descending dependence order. An examination of the individual constituents reveals that every pair has one stock from the “Industrials” sector most frequently paired with either a “Materials” one (5 pairs), or with an “Information Technology” stock (3 pairs). Furthermore, in all ten pairings an examination of the companies suggests that the dependence is not really surprising – for example, the strongest is between

3 Visualizing dependence in high dimensions with zenplots

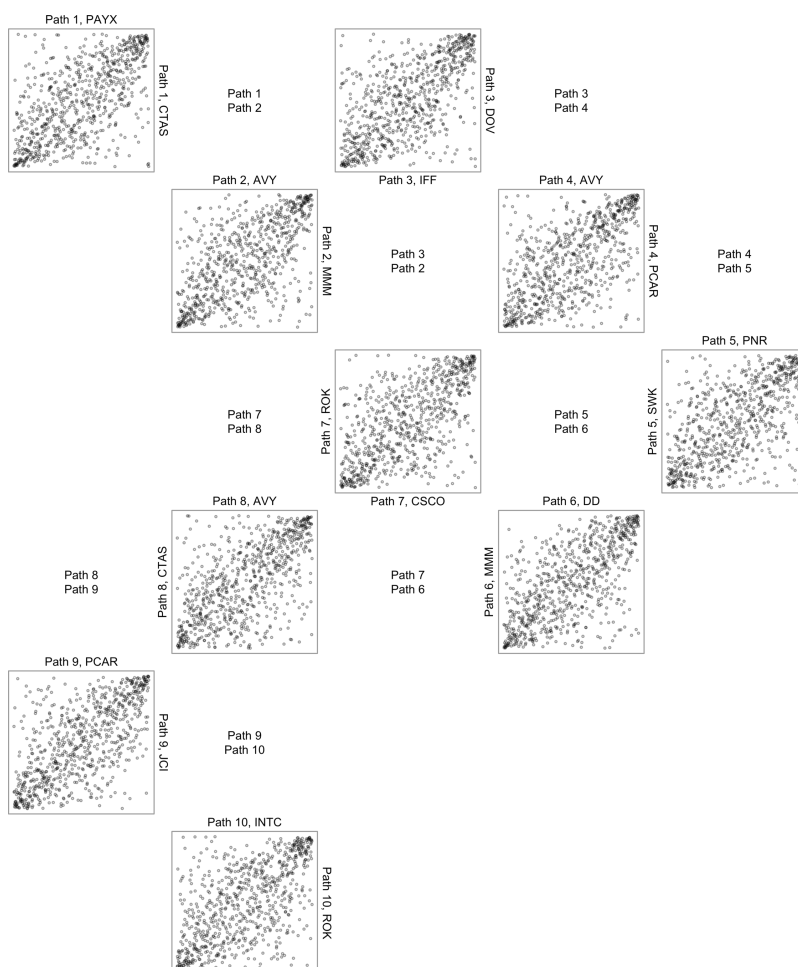


Figure 7 A zenplot constructed from a zenpath displaying the pseudo-observations of those 10 pairs of variables with largest upper tail-dependence coefficient which belong to different GICS business sectors.

PAYX a provider of human resource outsource services from the “Information technology” sector and CTAS from the “Industrials” sector that provides such “diversified support services” as corporate identity, promotional services, restroom cleaning, and supplies, and the weakest dependence of the ten is between Intel Corp. (INTC, “Information Technology”) and Rockwell Automation Inc. (ROK, “Industrials”).

Note that there are as many paths in Figure 7 as there are pairs displayed. Although some constituents appear more than once (for example, AVY Avery Dennison Corp. (3), CTAS Cintas Corporation (2), MMM 3M Company (2), PCAR PACCAR Inc. (2), and ROK Rockwell Automation Inc. (2)), nowhere along the zenpath of decreasing upper tail dependence is one of the repeated constituents shared by consecutive plots.

Looking again at Figure 6, we see that only three sectors appear in the top ten strongest dependencies, namely “Consumer discretionary”, “Energy”, and “Financials”. This misses seven out of the ten GICS sectors. We might ask, then, what pair of constituents within each and every sector has the largest upper tail dependence?

Figure 8 shows a zenplot of the ten GICS sectors (in alphabetical order as before) as ten separate zenpaths labelled GICS 1–GICS 10. Within each sector, the constituent pairs are sorted from greatest to least dependence.

The first plot in the path of each sector in Figure 8 displays the pseudo-observations for that pair of constituents having the largest upper tail-dependence coefficient within that sector. For each sector, the zenpath beginning at that pair continues in decreasing tail dependence as long as the path is connected; it ends as soon as the path ends in that sector. For example, within the first GICS sector (“Consumer discretionary”) only one pair appears, as no connection to the next pair within that sector can be made according to the zenpath of decreasing tail dependence; this is why the strong relation between the FOX and FOXA shares of Figure 6 does not also appear in Figure 8. However, the second sector (“Consumer staples”) the two pairs with strongest tail dependence share the variate PG (Procter & Gamble) and so appear as a connected pair joining three well known companies (from two different sub-sectors) offering personal and household products (viz. KMB (Kimberly-Clark), PG, and CL (Colgate-Palmolive)).

The concatenated zenpaths of Figure 8 separate the groups visually and give some sense of their size. The groups, their stocks in order, and the sub-sectors to which they belong are as follows: GICS 1 or “Consumer discretionary” (CMCSK and CMCSA, both Comcast); GICS 2 or “Consumer staples” (KMB (Kimberly-Clark), PG (Procter & Gamble), and CL (Colgate-Palmolive) from two closely related but different personal or household product sub-sectors); GICS 3 or “Energy” (XOM (Exxon), CVX (Chevron), COP (ConocoPhillip), from two closely related but different oil & gas sub-sectors); GICS 4 or “Financials” (VNO (Vornado), EQR (Equity residential), SPG (Simon Property group), PSA (Public Storage), and VNO again, all “REITs”); GICS 5 or “Health care” (ANTM (Anthem Inc.), AET (Aetna), CI (CIGNA Corp.) , and ANTM again, all “Managed health care”); GICS 6 or “Industrials” (NSC (Norfolk Southern), UNP (Union Pacific), CSX (CSX Corp.), all “Railroads”); GICS 7 or “Information technology” (XLNX (Xilinx Inc.), ALTR (Altera Corp.), both “Semiconductors”); GICS 8 or “Materials” (PX (Praxair), APD (Air products and chemicals), both “Industrial

3 Visualizing dependence in high dimensions with zenplots

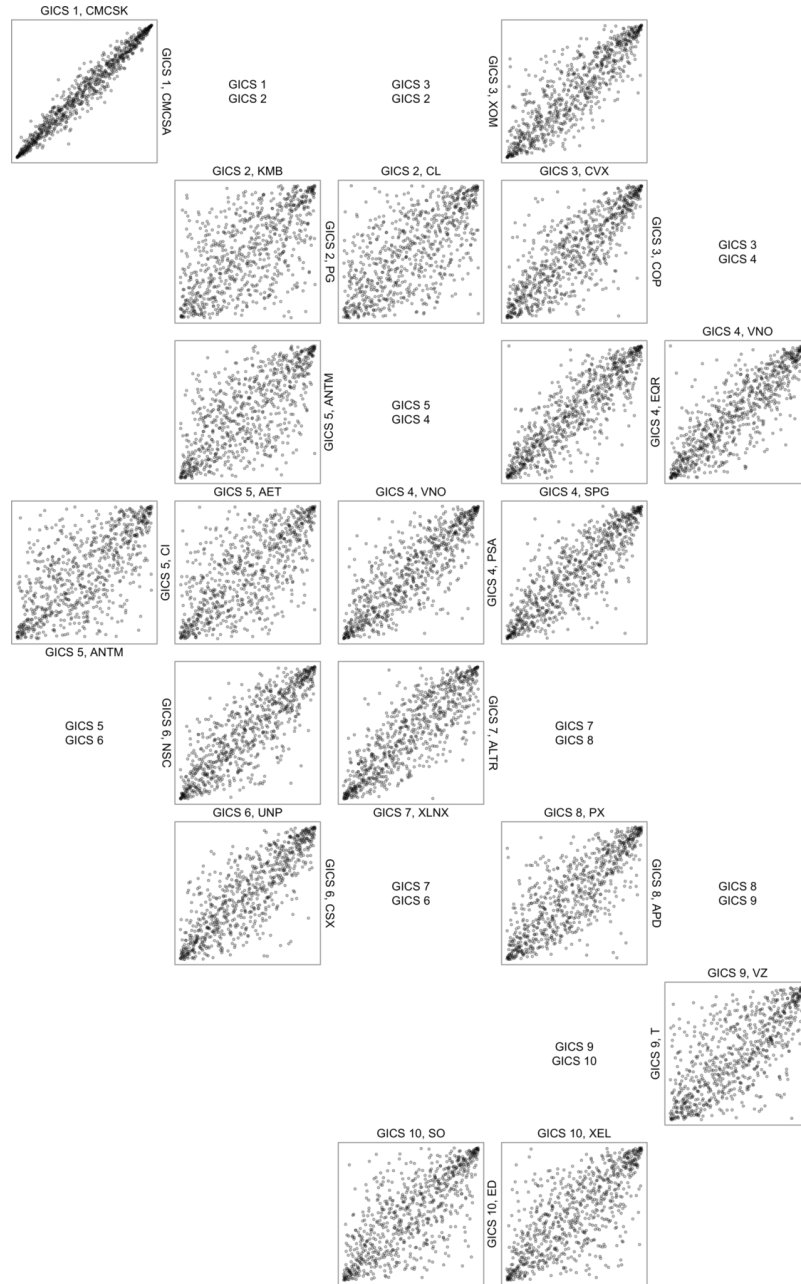


Figure 8 A zenplot constructed from a zenpath displaying the pseudo-observations of those groups of connected pairs of constituents with largest upper tail-dependence coefficient within each GICS business sector; the latter (in alphabetical order) are labelled GICS 1–GICS 10.

gases”); GICS 9 or “Telecommunication services” (VZ (Verizon), T (AT&T), both “Integrated telecom services”); and GICS 10 “Utilities” (XEL (Xcel Energy Inc.), ED (Consolidated Edison), SO (Southern Co.), two “Electric utilities” one “MultiUtilities”). The zenplot has clearly picked out some interesting related groupings with many of the strongest relations within a sector also appearing within the same (or closely related by definition) sub-sector.

Clearly some sectors show much weaker within-sector dependence than do others. We could continue in this way, using zenplots to more deeply explore dependence within or between sectors and sub-sectors. Instead, we now turn our attention to how zenplots might also be used in assessing the models we are using.

4 Model assessment

Zenplots can be used to quickly arrange nearly any visual display in a compact but informative way. Here we illustrate how zenplots, as well as some other displays, might be used in the very important task of model assessment.

4.1 Checking serial dependence of the marginals

We modelled each component series of negative log-returns by an ARMA(1, 1)–GARCH(1, 1) model with serially (or temporally) independent t innovations. The assumption of serial independence might be assessed visually via the autocorrelation function (ACF) of the standardized residuals $\hat{Z}_{t,j}$, $t \in \{1, \dots, T\}$, $j \in \{1, \dots, d\}$.

Figure 9 shows the ACFs up to lag 30 of sixteen standardized residual series. The order of these series is chosen to place earliest in the sequence those components which most challenge the null hypothesis of serial independence. We measure the strength of this challenge as follows. For each component, the Ljung–Box test statistic is computed for every lag from 1 to 30. Because, under the null hypothesis, the magnitude of this statistic increases with the lag, the p-value for that lag’s test statistic is used to place the different lag test statistics on a common scale (that is, ordering by test statistic magnitude does not make sense here since the different lags will have different magnitude test statistics each with its own distribution when the hypothesis of serial independence holds). The smallest of these p-values corresponds to that lag which most greatly challenges the hypothesis of serial independence for this component as measured by a Ljung–Box test. The components are then ordered from smallest to largest by these minimal p-values; Figure 9 shows the ACFs for the first sixteen (most challenging) components in this order.

Another way in which the null hypothesis of serial independence might be violated is if there were some remaining temporal dependence in the volatility. To assess this, we apply the same strategy as above to challenge the null hypothesis of serial independence except that now, since interest lies in volatility, we use the series of squared estimated standardized residuals $\hat{Z}_{t,j}^2$, $t \in \{1, \dots, T\}$, for each component j when conducting the Ljung–Box tests. Figure 10 shows the ACFs for those 16 components j having the smallest p-values over all components and, for each component, over all Ljung–Box tests for lags 1 to 30. As was the

4 Model assessment

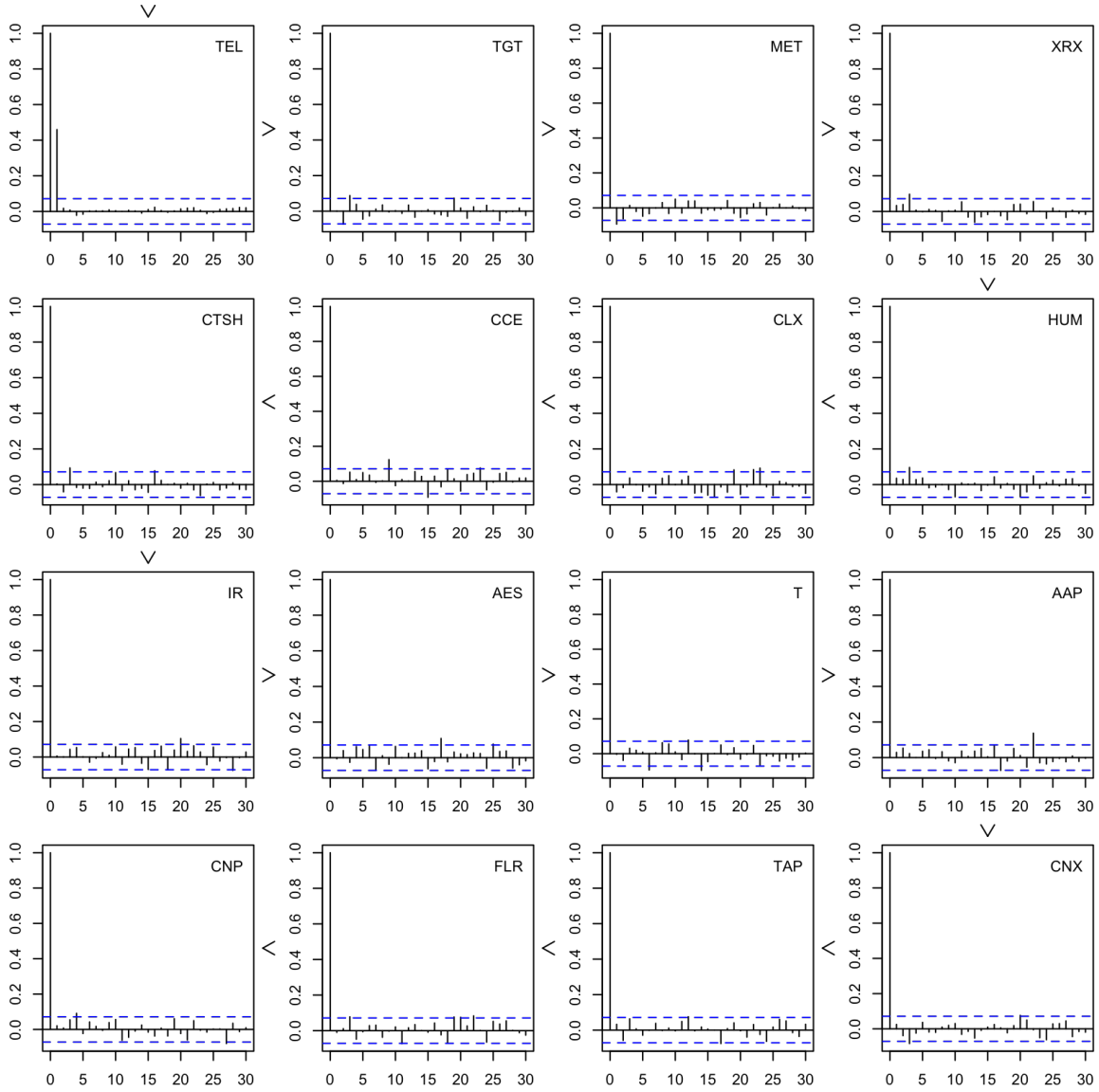


Figure 9 A zenplot of ACFs of those 16 standardized residual series with largest maximal (over lags 1 to 30) Ljung–Box test statistics.

4 Model assessment

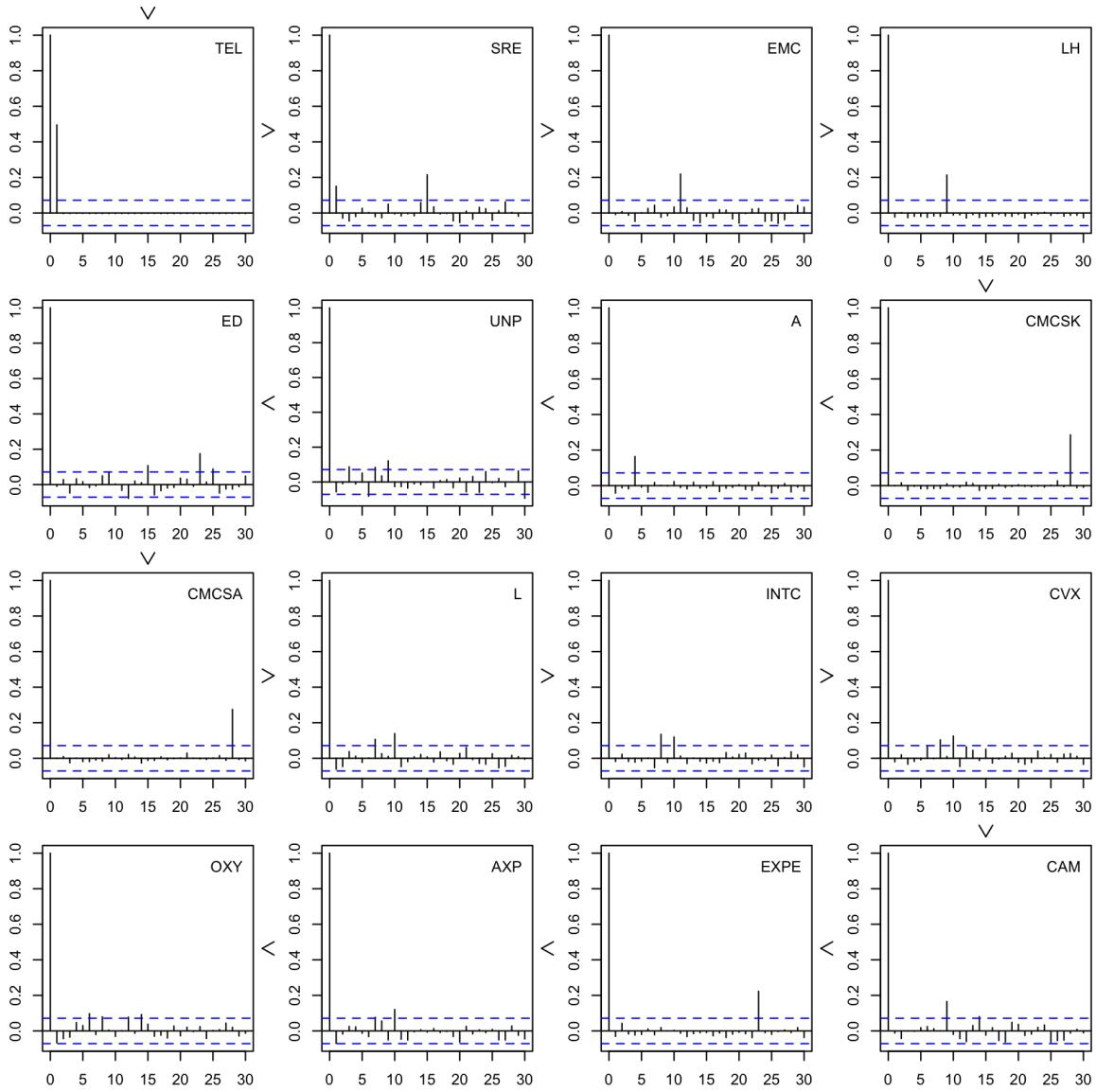


Figure 10 A zenplot of ACFs of those 16 squared standardized residual series with largest maximal (over lags 1 to 30) Ljung–Box test statistics.

case in Figure 9, the component most challenged by possible serial dependence is TEL; all remaining components in Figure 10 differ from those which appeared in Figure 9.

Together, then, the zenplots of Figures 9 and 10 serve up the ACF displays of those components that demonstrate the greatest challenges to serial independence (in level or volatility), at least as measured by the minimum p-value of a Ljung-Box test for every lag from 1 to 30. That is, by this particular measure, in each Figure these are the strongest 16 cases against the null hypothesis for all 465 components. An examination of these ACFs reveals little serial dependence with one notable and jarring exception. Appearing as the first (and strongest) case in each zenplot, the ACF of the component TEL (TE Connectivity Ltd.) shows a significant lag 1 auto-correlation where none should exist (since these are the auto-correlations of the estimated standardized residuals from an $\text{ARMA}(1, 1) - \text{GARCH}(1, 1)$ model).

To see how this might have occurred, in Figure 11 we plot the standardized residuals

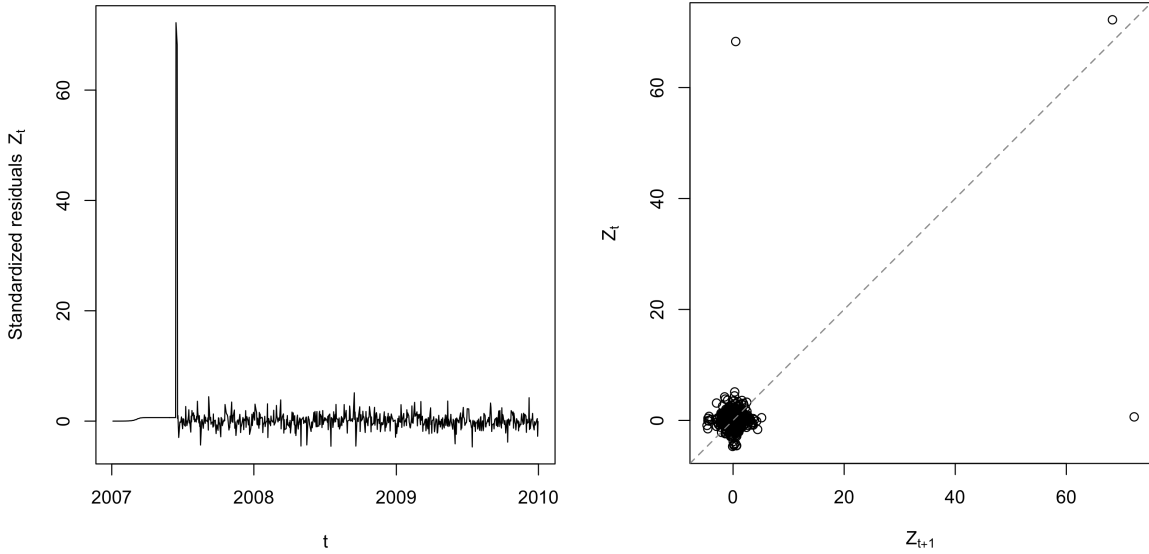


Figure 11 The standardized residuals from fitting a marginal $\text{ARMA}(1, 1) - \text{GARCH}(1, 1)$ model to TEL (TE Connectivity Ltd.) plotted at left over time and at right against the values in the immediately previous time period (a lag 1 plot).

over time for the component TEL (the left display) together with their lag 1 plot (the right display). Two adjacent huge positive residuals appear near the beginning of the series. Their adjacency is perhaps clearer in the lag plot, where a single point appears in the top right corner as a result. This single point is far enough away from the bulk of (essentially uncorrelated) points in the bottom left of the lag plot to have induced the spurious auto-correlation. Of course, had we not examined the zenplot for the strongest ACFs (as determined by the minimum p-value over the several Ljung-Box tests for each) over all components, this spurious auto-correlation might never have been discovered.

4 Model assessment

Recall that TEL is one of four components of the 465 fitted that had missing data at the beginning of their series, and that these were filled in by the first non-missing value (see Figure 1). One of these (TWC; Time Warner Cable) had very few missing cases; the two remaining (DAL for Delta Air Lines and DFS for Discover Financial Services) had about as many filled in as had TEL. An examination of the standardized residuals for DAL and DFS showed a single enormous (several orders of magnitude) positive residual at the first observed (that is, non-filled) value in each series; there was no corresponding outstanding standardized residual estimated for TWC. Because each of DAL and DFS had only a single outlying estimated residual, neither component showed up in the strongest ACFs; the corresponding lag 1 plots resembled that of Figure 11 except that no point appeared in the top right corner and hence no spurious auto-correlation. It would seem that the problem is an artefact of the fitting mechanism `ugarchfit()` from version 1.3-6 of the `rugarch` package together with the fact nearly the first 20% of the series is constant (due to filling in missing values). It is curious however, that `ugarchfit()` produced *two consecutive* large residuals in the case of TEL, but only a single gigantic residual for each of DAL and DFS. A. Ghalanos (maintainer of `rugarch`) suggests that the problem lies in the number of constant values at the beginning of each series (personal communication). Whatever the reason for this peculiarity in the fitting, it might easily have gone unnoticed had we not considered the zenplots of Figures 9.

The zenplots of Figures 9 and 10 show that the sixteen ACFs which most challenge the hypothesis of serial independence provide little evidence against the hypothesis of serial independence. Other than the spurious lag one autocorrelations, the remaining autocorrelations are mostly quite small, especially for the standardized residuals of Figure 9. For the volatility, a few series of Figure 10 show the occasional lag beyond the 95% limits for uncorrelated data (given by the horizontal dashed lines). On the basis of these plots, a more complex GARCH component for these individual series might be considered, perhaps depending on the component involved, but care needs to be taken to not over interpret the significance of the observed departures. They were, after all, selected as the most challenging cases (via 30 Ljung-Box tests) from 465 components; the putative 5% level given by the horizontal lines is a gross understatement of the actual observed level of significance. Given the paucity of evidence against the hypothesis of serial independence, and since our primary modelling goal here is to model the dependencies *between* components, we will continue our investigation using the common and parsimonious $\text{ARMA}(1, 1) - \text{GARCH}(1, 1)$ for each of the 465 components. That is, we proceed based on our interpretation that these “worst-case” plots show little evidence against the null hypothesis of serial independence in the estimated standardized residuals; more complex modelling of any remaining serial dependence structure will not be pursued.

Remark 4.1

It is important to note that the plots of Figures 9 and 10 are constructed from zenpaths which, as with earlier plots, rely on some measure of each plot’s importance to determine its order along any zenpath. These particular figures used the minimum p-value from several

Ljung–Box test statistic to provide the ordering. Unlike the test statistic itself, the p-value has the advantage that all plots are then compared using a common scale.

However, it is important to note that using the p-values to provide order is not the same as reporting them as the observed level of significance when testing the hypothesis of serial independence anywhere in the series. Because many tests are involved the actual significance level is necessarily larger than the smallest p-value, which was used here. After all, the p-value reported by each test assumes that it is the only test conducted. In contrast, when constructing the zenplots a great many tests were conducted and only the smallest p-values selected and reported (in this case from more than 13,000 tests!). A true observed significance level must take into account this multiple testing. Determining how best to adjust the p-values so that they might accurately represent the true significance level is not always obvious, especially in this case. For example, the adjustment here would need to account for the fact that first the minimum value is taken over 30 (not necessarily independent) tests, and then the minima of these minima is then taken over the 465 separate components. Adjusting the p-value to better reflect the true significance level is likely to be a challenge in this case, and in general for many other cases where plots are ordered.

Fortunately, for the purpose of determining a zenpath ordering to be presented for display, the ordering provided by the (uncorrected) p-values is sufficient and will, in most cases, provide the same ordering as would the true observed significance levels. For this reason, wherever p-values are used to order plots it would be best to omit reporting the values so as not to mislead the viewer. \square

4.2 Checking the marginal distributions for being t

We now turn to the model assumption of having t innovations. This assumption can be assessed visually via a quantile-quantile plot (or Q-Q plot) of the sample quantiles of the standardized residuals.

Figure 12 shows Q-Q plots for sixteen components. The vertical axis of each Q-Q plot marks the sample quantiles and the horizontal axis marks the theoretical quantiles for a standardized t distribution with degrees of freedom estimated from the sample (displayed as $\hat{\nu}$ in the plots). The grey regions are point-wise empirical confidence envelopes for each quantile as constructed from 1,000 samples (each of size $n = 755$) generated from a t marginal on the estimated degrees of freedom $\hat{\nu}$. From darkest to lightest, the regions correspond to the central 90, 95, and 99% of the simulated sample quantiles as well as the range of all 1,000 generated. Departures from the marginal $t_{\hat{\nu}}$ hypothesis are seen as points appearing at the extremities (or outside) of the given grey regions; see Oldford (2016) for details. The sixteen components chosen were those with largest Anderson–Darling test statistic, that is, the zenpath is the path of decreasing evidence against the null hypothesis that the marginal ARMA(1, 1) – GARCH(1, 1) residuals follow a standardized $t_{\hat{\nu}}$ distribution with estimated degrees of freedom $\hat{\nu}$.

The first three stocks TEL (TE Connectivity Ltd.), DFS (Discover Financial Services), and DAL (Delta Air Lines) thus display the strongest evidence against the null hypothesis.

4 Model assessment

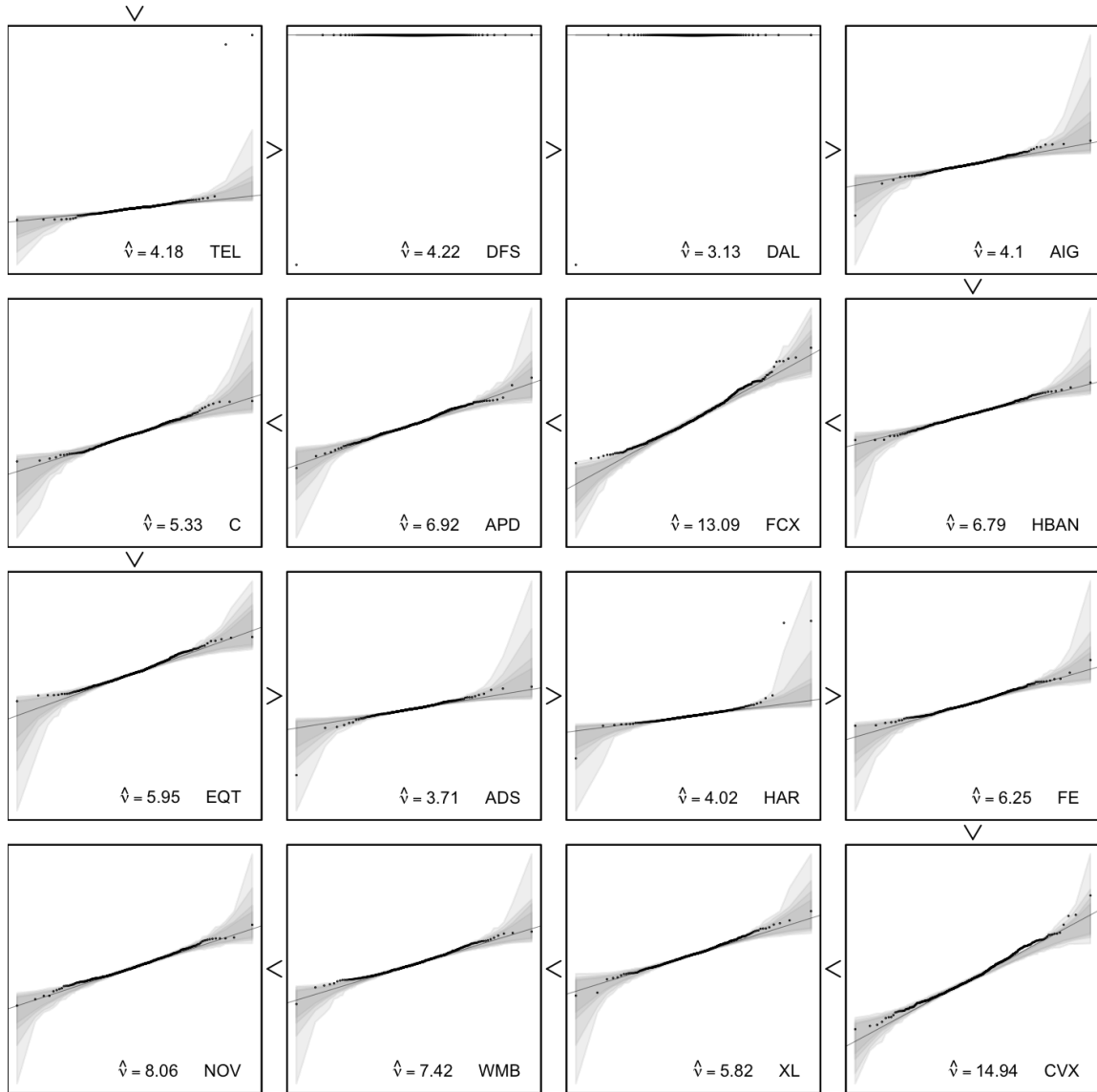


Figure 12 A zenplot of Q-Q plots for those 16 margins having the largest Anderson–Darling test statistics; the fitted degrees of freedom (\hat{p}) are as indicated in each plot. The line of exact agreement (the $y = x$ line) appears as a fine line in each plot.

This is perhaps not too surprising in light of the discussion surrounding the ACF plots of Figures 9 and 10 as well as the residual plots of Figure 11. There we found that TEL had two large standardized residuals that caused a spurious lag 1 autocorrelation. These now both appear again as the pair of large positive residuals in the first Q-Q plot of Figure 12. The next two Q-Q plots bring attention to the massive singleton outliers of DFS and DAL which, as reported earlier, are likely to be artefacts of the `ugarchfit()` fitting mechanism for series whose first values are all identical. Again, by examining the zenplot of Figure 12 these difficulties are immediately brought to the attention of the analyst.

Similarly, it should be no surprise that AIG (American International Group) shows up next in order as not having a t innovation distribution. During the subprime mortgage crisis of 2008 AIG stock collapsed and would have failed entirely had it not been bailed out. This is picked up visually by the Q-Q plot as several of the positive standardized residuals are outside the range of the simulated envelopes on the right where the envelope is tight, just before it fans out.

It is interesting to note that the Anderson–Darling test statistics used to order the Q-Q plots in Figure 12 change abruptly in the supposed (uncorrected) p-values which they report. This is the case, for example, after the first four plots appearing in the top row, at HBAN (Huntington Bancshares) along the zenpath.

In contrast, several of the remaining Q-Q plots clearly show evidence against the hypothesis of the t marginal (with those estimated degrees of freedom $\hat{\nu}$) For example, HAR (Harman International Industries, Inc.) and ADS (Alliance Data Systems, Inc.) have outlying standardized residuals, while FCX (Freeport-McMoRan), C (Citigroup, Inc.), EQT (EQT Corp.), CVX (Chevron Corporation), and WMB (Williams Companies, Inc.) each suggest some asymmetry.

Graphical methods are able to detect many different types of departures and, with zenplots it actually becomes feasible to view at least the most interesting ones among 465 Q-Q plots. Some other measure based entirely on the geometric features of the Q-Q plot might even be more helpful in choosing an interesting zenpath than this Anderson–Darling test.

Remark 4.2

In constructing the zenplot of Figure 12, the value of the Anderson–Darling test-statistics were used to order the plots. Generally, ordering by the p-value is preferred but is equivalent to ordering by the test statistic in this particular case. The reader is again cautioned that any such p-values would need to be corrected before being interpreted as observed levels of significance. In addition to the problems of multiple testing mentioned in the earlier remark, to arrive at the correct level of significance, adjustment would also need to consider the effect of using degrees of freedom for the t distributions that themselves are uncertain since they too must be estimated from the data.

Again, the (uncorrected) p-values are used to determine an order in which to lay out the plots, beginning from those most likely to show evidence against the hypothesis (by this measure) to those least likely. Perhaps, as the above analysis suggests, had we some measure

of departure from the distributional hypothesis based only on the geometric configuration of a Q-Q plot, we might use that measure to order the plots – without any knowledge of what the corresponding level of significance might be. The zenpath would serve up those plots which were of interest according to this measure. \square

4.2.1 Zenplot layout

Some important features of zenplot construction enabled the compact layout of Q-Q plots as in Figure 12 and make practical viewing of all 465 plots possible.

First, a zenplot is actually a layout of an alternating sequence of single coordinate and two-coordinate plots; in Figure 12 the alternation is between a “V” arrow shape (one dimensional location indicating an order) and a Q-Q plot (having two coordinates to be plotted).

Second, the location of each plot is determined by where it appears in a sequence of “direction” indicators, one of “u”, “d”, “l”, or “r”, for “up”, “down”, “left” or “right”; each one is the directive for where the *next* plot will appear relative to the present plot. The plots of Figure 12 begin as the top left “V” drawn to indicate “d” for the relative position of the first Q-Q plot. It then follows a series of eight “r” directions to move across the page alternating Q-Q plots and arrows, then two “d” to place the arrow down and to position the following Q-Q plot down on the next row. This Q-Q plot exits left (direction “l”) to start the sequence moving leftward back across the page. The zenplot thus zigzags back and forth across the page moving down when the edge of the page is reached and then reversing the horizontal direction. The zenplots of all previous figures were constructed using a slightly more complex sequence of directions; see the demo `SP500` for the corresponding source code. By using an appropriate sequence of directions, essentially any layout pattern of alternating plots can be constructed with a zenplot (for example, a spiral; see `?zenplot` for more details and additional features not described here).

Third, there is no restriction on the plots that may be drawn. The Q-Q plot used in Figure 12, for example, is not from the `zenplots` package of Hofert and Oldford (2016) but from `qqtest` of Oldford (2014). If a plot can be drawn in any one of three R plotting systems of `graphics`, `grid` (including `ggplot2`), or `loon`, it can be part of a zenplot.

4.3 Comparing models

In modelling high dimensional data, we have seen how zenplots are useful for both model interpretation and for model assessment. When we have different but competing models available, more direct comparisons of the fitted models can lead to deeper insight both about the dependence characteristics of the data and about the relative merits of the models. Again, zenpaths and zenplots can be put to good use in this sort of analysis for high-dimensional data.

To be concrete, the approach taken so far has been very flexible, in that it allows separate t copula models for every pair of variates (an even more flexible nonparametric approach is

4 Model assessment

sketched in Appendix A). This is sensible if we are only interested in the notion of bivariate tail dependence. It might be argued, however, that there should be a single multivariate model fitted, one that is designed to incorporate all 465 dimensions simultaneously.

One natural candidate to compete with a collection of pairwise t copula models would be a multivariate t copula. It is also known to have fit multivariate financial return data fairly well and can actually be fit to our high-dimensional data. To fit the multivariate t copula model we use the fitting procedure of Mashal and Zeevi (2002); see more recent versions of the R package `copula` of Hofert et al. (2017).

In Section 4.3.1, tail dependencies of the fitted multivariate t model are compared to those of the previous collection of pairwise fitted t copulas. Zenpaths derived from comparisons between these two fitted types of models identify important differences in the tail-dependence estimates; the corresponding zenplot presents the component pairs for further examination. In Section 4.3.2, we use differences in the pairwise fits of these models as measured by another Anderson–Darling test statistic to identify pairs where shared model assumptions might be suspect. The possibility of other measures of interest is raised in Section 4.3.3.

4.3.1 Tail dependence

As with the pairwise modelling, this fully joint model will have correlation parameters from whose estimates, via Equation (3), an estimate of the upper tail dependence for any pair of returns can be obtained. These measures from the full model can then be examined as before.

Figure 13, is the equivalent of Figure 5, except now the $\hat{\lambda}$ s have been estimated from

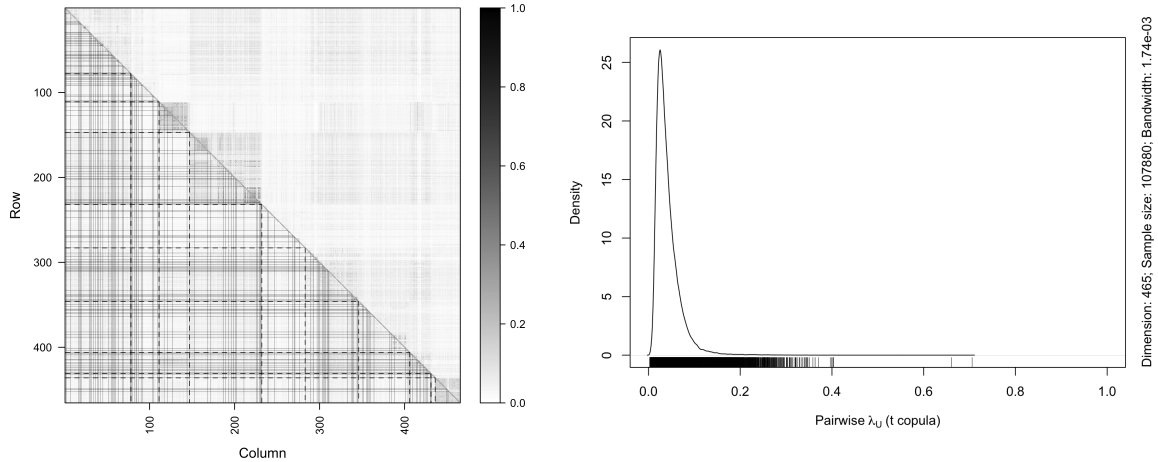


Figure 13 Matrix of implied upper tail-dependence coefficients as obtained from a fitted joint t copula (left-hand side); the fitted degrees of freedom were 12.98. Density plot of the corresponding $\binom{465}{2}$ entries (right-hand side).

the *full* 465-dimensional, t copula model. The matrix display at left is similar in pattern

4 Model assessment

to its counterpart from Figure 5. The most dramatic difference between the two is that the matrix of Figure 13 looks like a washed out version of that of Figure 5, that is, the full model overall suggests weaker pairwise upper tail dependencies than do the separate pairwise models. Comparing the two densities of the two sets of estimates from the right hand displays of Figures 5 and 13, we see that the full model has reduced the range of the bulk of the dependence estimates from less than 0.3, to less than 0.1.

Matching corresponding estimates of λ from the two models, we can compare their values more directly. Figure 14(a) displays the density of their differences showing that the

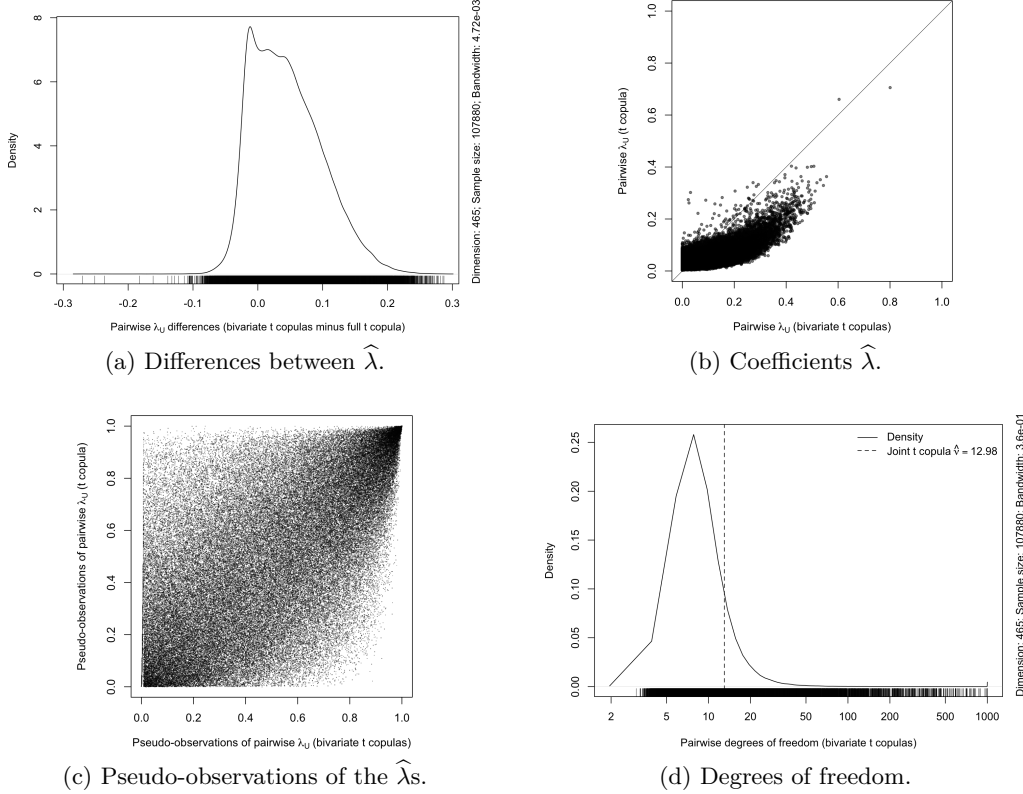


Figure 14 Comparing estimates: joint t copula and the separate pairwise t copula models.

estimates from the separate pairwise models are typically larger (often by more than 0.1) than those from the joint model. Figure 14(b) plots these estimates as pairs; the points lying below the $y = x$ line are cases where separate pairwise modelling estimates larger upper tail dependencies than does the joint copula model. Dependence between the two sets of upper tail-dependence coefficient estimates is summarized by the pseudo-observations from the upper tail-dependence coefficients plotted in Figure 14(c) which suggest an asymmetric dependence.

With different estimates of the upper tail-dependence coefficients arising from the two

4 Model assessment

fitted models, it might be of interest to examine which pairs of components have given rise to the greatest differences. Figure 15 shows the zenplot of the twenty component pairs

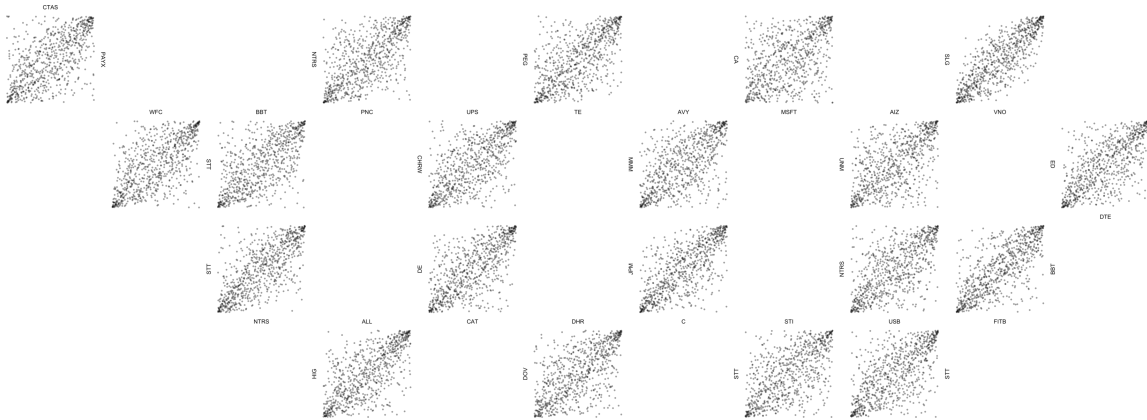


Figure 15 A zenplot of 20 component pairs whose difference in upper tail-dependence estimates are greatest between a pairwise t copula and a 465 dimensional multivariate t copula. Components are sometimes from the same sector, sometimes from different sectors.

having the greatest absolute difference in upper tail-dependence coefficients.

We might also investigate the difference in estimated degrees of freedom from the two models. The density of the degrees of freedom from the pairwise models is shown in the right-hand plot of Figure 14; the single estimated degrees of freedom of the full t copula, 12.98, is shown as the vertical line. As can be seen, the pairwise models suggest heavier tails (lower degrees of freedom) in general than does the joint model. The dramatic restriction on the degrees of freedom forced by the full model seems to force lighter tails on most of these pairwise t copulas.

Unconstrained, the degrees of freedom from the pairwise fits are highly variable and, for the most part, lower than that estimated by the full model. As with the estimated coefficients of upper tail dependence, a zenplot could be constructed for those pairs of components where the difference in the estimated degrees of freedom is largest, or, given that tail dependence is of primary interest, perhaps just those pairs having the smallest estimated degrees of freedom in the pairwise models. The zenplot of the latter shares many of the same pairs as those shown in Figure 15 and so is not produced here.

Instead, in the next subsection, we introduce another measure based on both types of models which will be used to produce another zenplot of interesting component pairs.

4.3.2 Comparing fits

Suppose we had a test that assessed the fit of a copula model on any pair of components. For every pair of components we could then test each of our models: the pairwise fitted

4 Model assessment

t copula models and the corresponding marginal models of the full multivariate t copula model. If one doesn't fit but the other does, then this suggests that the degrees of freedom and correlational structure of one model better describes this pair of components than does the other; there would seem to be no evidence against the distributional shape in this case. However, if *neither* fit well then it might reasonably be asserted that the distributional family is sufficiently suspect that a plot of the pseudo-observations for this pair should be examined. A zenplot of all component pairs where both types of models fit poorly might therefore be of interest to an analyst.

Such a test can be constructed as an Anderson–Darling test based on observations derived from (a function of) the transformation of Rosenblatt (1952) of the pseudo-observations common to both models. In each case, the transformation will be derived from the hypothesized copula model. The derived observations are constructed as follows. For a random vector $\mathbf{U} \sim C$ for some copula C , we can transform $\mathbf{U} = (U_1, \dots, U_d)$ to \mathbf{V} as

$$\begin{aligned} V_1 &= U_1, \\ V_2 &= C_{2|1}(U_2 | U_1), \\ &\vdots \\ V_d &= C_{d|1, \dots, d-1}(U_d | U_1, \dots, U_{d-1}), \end{aligned}$$

where, for $j \in \{2, \dots, d\}$, $C_{j|1, \dots, j-1}(u_j | u_1, \dots, u_{j-1})$ denotes the conditional probability that $U_j \leq u_j$ given $U_1 = u_1, \dots, U_{j-1} = u_{j-1}$. This embeds the conjectured copula in the calculations and, following Rosenblatt (1952), the transformed random vector \mathbf{V} will follow a $U(0, 1)^d$ distribution if and only if the copula C is correct; note that the construction depends on the order of the variates in the Rosenblatt transformation. Any mapping $g : [0, 1]^d \rightarrow \mathbb{R}$ will produce a random variable $W = g(\mathbf{V})$ whose distribution, if known, may be tested via an Anderson–Darling test.

For illustrative purposes, we choose $W = \sum_{j=1}^d (\Phi^{-1}(V_j))^2$ where Φ is the standard normal distribution function. If C is correct, $W \sim \chi_d^2$ and so could be assessed using the realizations w_1, \dots, w_T . Unfortunately, the realizations w_1, \dots, w_T are not directly available and the estimated realizations $\hat{w}_1, \dots, \hat{w}_T$ must be used in their place. Clearly the latter will not be independent χ_d^2 realizations though they may be good enough for this purpose (as suggested, for $d = 2$, by Breymann et al. (2003); the limitations of this tests are known well, see, for example, Dobrić and Schmid (2007)). When interest lies only in pairs of components, then we could use each fitted copula model as the hypothesized copula for the Rosenblatt transformations on each pair to determine putative χ_2^2 (estimated) realizations, and hence an Anderson–Darling test, for each copula on every pair.

Anderson–Darling tests were constructed in this way and applied to all 107,880 pairs of components, once using the fitted pairwise t copulas and once using that corresponding bivariate margin of the full multivariate t copula. For pairs with small p-values in both cases, the choice of the t family may be a problem (and not just the common degrees of freedom assumed by the full model, for example). For pairs of returns with rather small

4 Model assessment

p-values when testing based on the full model but rather large p-values for the pairwise model, a bivariate t copula may be an adequate model for each of these pairs but not a full t copula model.

Figure 16 lays out the pseudo-observations of those pairs of standardized residuals with smallest p-values for the Anderson–Darling test for the bivariate t copula models. Note that all pairs until and including DFS and DAL in the last row of the zenplot are precisely those for which the order is the same as for the p-values for the bivariate t copulas implied by the full t copula model. Furthermore, whenever adjacent plots share variates they are displayed in the same group (as determined by `connect_pairs(, duplicate.rm = TRUE)`). The pseudo-observations may now be critically examined by an experienced analyst to determine how each pair of standardized residuals appears to depart from a t copula and to possibly even suggest an alternative copula family. Note that this is not an easy task as replacing a bivariate model by another one can (and most often will) not lead to a proper multivariate model anymore; however, the information on *how* the data departs from the hypothesized model is valuable in making a decision whether the latter is still acceptable for the modelling task at hand.

A visual inspection can reveal departures other than those identified by the test statistic used to select the plot. For example, Anderson–Darling emphasizes departures in the hypothesized distribution’s tails. The hypothesized distribution here, however, is χ^2_2 (albeit derived from a hypothesized t copula). The right tail of this χ^2_2 is constructed from large *and* small pseudo-observations and so does not necessarily identify a difference between the upper-right and lower-left of the plots of pseudo-observations. Rather, these two tails of the bivariate t copula are treated together, as one, in the assessment. Even so, examination of the plots of Figure 16 does reveal several showing an apparent asymmetry between the two densest corners, a well-known stylized fact of financial data not captured by a t copula. Asymmetry in the other direction can also be detected visually in several plots.

Similarly, the left tail of this χ^2_2 is constructed from pseudo-observations near 1/2 and so this Anderson–Darling test will emphasize differences from the centre of a t copula. Unusual spaces and/or densities in the centre of the plots might therefore be detected by this test. Indeed, the last plot (bottom-leftmost plot) of Figure 16 shows an extremely unusual central configuration. The returns involved are those of DAL and DFS which were also previously identified by the Q-Q plots of Figure 12. These were two of the three stocks that were missing many measurements early in the time period under study. This would seem to corroborate the value of the Anderson–Darling test on the middle part of the copula. Unfortunately, when the third incomplete stock, TEL, is plotted against either of DAL or DFS, the pseudo-observations also reveal strong linear (non t copula) patterns at the centre. Yet, neither plot is highlighted by Anderson–Darling.

Another problem with our use of the Anderson–Darling test revealed is numerical. Of the plots of Figure 16, all until that of DAL and DFS have the same calculated p-value. This is because the squared normal probability integral transform for some of the putative uniforms actually returned `Inf` in R. This may not be such a problem for purposes of identifying pairs that are not t copulas, but it severely diminishes the utility of an ordered layout provided by

4 Model assessment

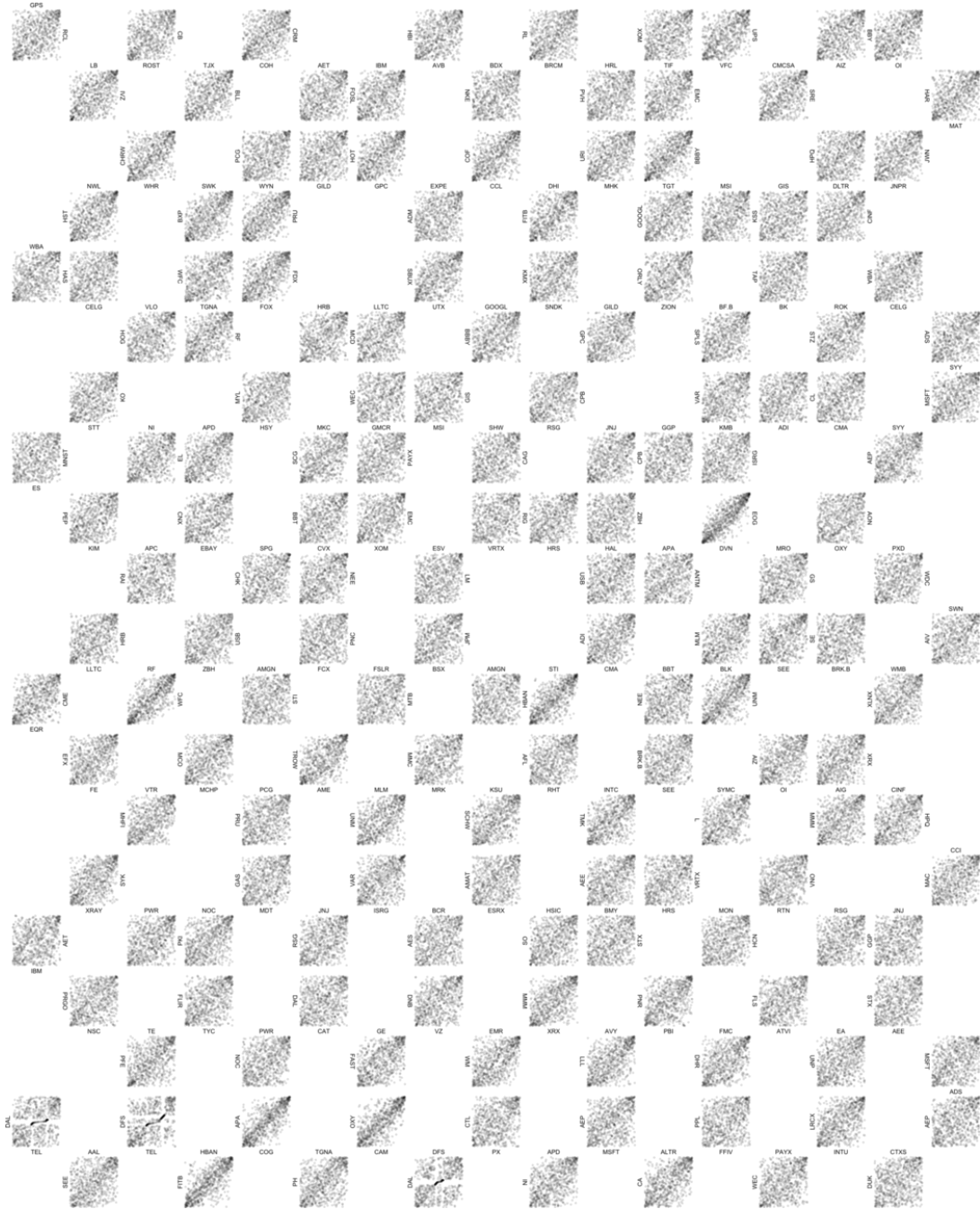


Figure 16 A zenplot constructed from a zenpath displaying the pseudo-observations of those pairs of variables with smallest p-value of the Anderson–Darling test for the bivariate t copulas. Note that all pairs until and including DFS and DAL (see last row) are precisely those for which the order is the same as for the p-values for the bivariate t copulas implied by the full t copula model.

zenplot. Those plots of Figure 16 are thus unordered with respect to one another (though they do properly precede the last one).

Other criticisms can and have been levelled at the Anderson–Darling test and, as noted earlier, it would be better were it replaced by a parametric bootstrap; see Dobrić and Schmid (2007) and Genest et al. (2009)). Besides the challenge of determining arbitrary values of the cumulative distribution function of a multivariate t , with non-integer degrees of freedom, the computational burden alone of a parametric bootstrap for all pairs of such high-dimensional data is currently prohibitive for practical purposes. In our problem, we have $d = 465$ yielding 107,880 bivariate pairs of $n = 755$ pseudo-observations. By our calculations, the computation required to determine p-values in this way, for this problem, is possibly only half the computation needed by Genest et al. (2009) to carry out their entire Monte Carlo experiment restricted to $d = 2$. And that, they report in 2009, “required the nearly exclusive use of 140 CPUs over a one-month period.”

4.3.3 Other measures

It is an important feature of a zenplot that all pairs may be filtered by some measure of interest so that only those pairs which matter are presented to the analyst for closer examination. And to this end, the Anderson–Darling test employed above can be of value, but can also be problematic as was just discussed. However, it would be better to have several such measures of interest, each detecting a different aspect of the data.

A zenplot could then be produced for every such measure and provide the analyst much more insight into the data. For general characteristics of a scatterplot, scatterplot diagnostics (or *scagnostics*) were introduced about 30 years ago by John and Paul Tukey and implemented more recently by Wilkinson et al. (2005). It is an interesting research problem to define analogous measures of interest but which are specific to copula modelling.

Even without such measures, for dimensions as high as $d = 465$ examined here, zenplots make it possible to actually examine all $\binom{d}{2}$ plots. The compactness of a zenplot is such that as many as 660 plots can be produced per page, giving about 164 pages of plots that serve at least as a visual record of the dependencies between returns. As proof of concept, we actually examined 107,880 plots using a standard PDF reader on screen in about 30 minutes. Even in this short of time, we were able to get a sense of the variety of patterns in the pairs and to visually identify the most unusual pairs (for example, any two of DAL, DFS, and TEL).

5 Conclusion and discussion

A zenplot is a zigzag-like structure which consists of pairwise (alternating one- and two-dimensional) plots. The typical (but not exclusive) use-case is where two consecutive pairwise plots share an axis, that is, a variate. A zenpath allows one to construct, in various ways, a path along pairs of variates which can then be laid out with a zenplot. One

particularly important way to construct a zenpath is to have measures of interest on each plot; then only those plots that are interesting can be presented in the zenplot.

Zenplots and zenpaths are useful, for example, for detecting and visualizing dependence in high-dimensional data when scatterplot matrices are too crowded, not meaningful, or when it is computationally infeasible to display all bivariate margins. We demonstrated such a case with S&P 500 constituent data from 2007 to 2009, thereby focusing on the notion of pairwise tail dependence.

Zenplots can equally well be used as graphical goodness of fit tools for detecting regions or dimensions of departure from the assumed model. In Section 4, a number of model assumptions were assessed graphically by examining the strongest departures as given by a variety of common measures.

We also compared an ensemble of pairwise models against a single high-dimensional model. For example, the zenplots composed of Q-Q plots allowed the marginal t distributions implied by both types of models to be assessed as well as whether the single degrees of freedom parameter (and thus a joint multivariate t model) was supported by the data. Wherever model selection methods lend themselves to a series of graphical displays, zenplots and zenpaths will permit the displays to be efficiently laid out in an ordered fashion.

Finally, we saw that zenplots can be customized in quite a flexible way. Besides providing one's own zigzag-like structure, groupings, and plotting functions, one can also provide another graphics systems (available are `graphics` (used here in this work), `grid` (and thus also `ggplot2`) and even `loon` plots (for dynamic interaction)); see the many examples on `?zenplot` for more details concerning these features.

Acknowledgments

We would like to thank the associate editor for detailed feedback and many helpful remarks. We would also like to acknowledge the support of NSERC through our Discovery grants.

A Tail dependence based on bivariate nonparametric estimators

Another estimator for upper tail dependence was suggested by Schmid and Schmidt (2007); see also Jaworski et al. (2010, p. 231). It is nonparametric and essentially a properly scaled conditional Spearman's rho computed from the top right corner of the bivariate distribution. Figure 17 shows the analogue plots to Figures 5 and 13 for this nonparametric estimator, where the top right corner is determined by the marginal 90% quantiles, that is, those pseudo-observations which fall into $[0.9, 1]^2$.

References

Breymann, W., Dias, A., and Embrechts, P. (2003), Dependence structures for multivariate high-frequency data in finance, *Quantitative Finance*, 3, 1–14.

References

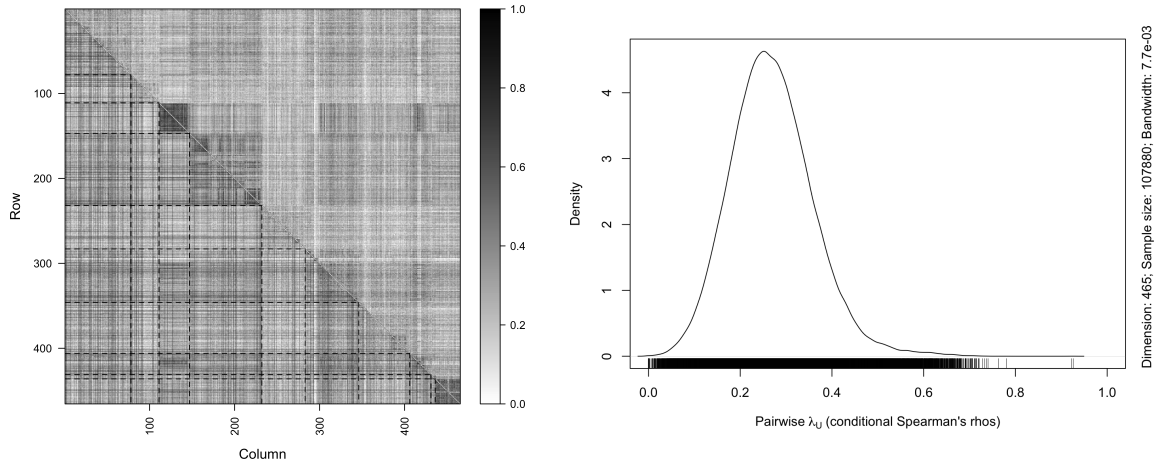


Figure 17 Matrix of pairwise upper tail-dependence coefficients as estimated nonparametrically by conditional Spearman's rho (left-hand side) and density plot of the corresponding $\binom{d}{2}$ entries (right-hand side).

- Demarta, S. and McNeil, A. J. (2005), The t Copula and Related Copulas, *International Statistical Review*, 73(1), 111–129.
- Dobrić, J. and Schmid, F. (2007), A goodness of fit test for copulas based on Rosenblatt's transformation, *Computational Statistics & Data Analysis*, 51, 4633–4642.
- Embrechts, P., Hofert, M., and Wang, R. (2016), Bernoulli and Tail-Dependence Compatibility, *The Annals of Applied Probability*, 26(3), 1636–1658, doi:10.1214/15-AAP1128.
- Genest, C. and Segers, J. (2010), On the covariance of the asymptotic empirical copula process, *Journal of Multivariate Analysis*, 101, 1837–1845.
- Genest, C., Rémillard, B., and Beaudoin, D. (2009), Goodness-of-fit tests for copulas: A review and a power study, *Insurance: Mathematics and Economics*, 44, 199–213.
- Ghalanos, A. (2011), rugarch: Univariate GARCH Models, R package version 1.3-6, (2016-06-23).
- Hofert, M. and Hornik, K. (2015), qrmtools: Tools for Quantitative Risk Management, R package version 0.0-6, (2016-06-23).
- Hofert, M. and Hornik, K. (2016), qrmdata: Data Sets for Quantitative Risk Management Practice, R package version 2016-01-03-1, (2016-06-23).
- Hofert, M. and Oldford, W. (2016), zenplots: Zigzag Expanded Navigation Plots, R package version 0.0-1.
- Hofert, M., Kojadinovic, I., Mächler, M., and Yan, J. (2017), copula: Multivariate Dependence with Copulas, R package version 0.999-14, (2017-02-09).
- Hurley, C. B and Oldford, R. W. (2010), Pairwise display of high-dimensional information via eulerian tours and hamiltonian decompositions, *Journal of Computational and Graphical Statistics*, 19(4), 861–886.

References

- Hurley, C. B. and Oldford, R. W. (2011a), Eulerian tour algorithms for data visualization and the PairViz package, *Computational Statistics*, 26(4), 613–633, ISSN: 1613-9658, doi: 10.1007/s00180-011-0229-5, <http://dx.doi.org/10.1007/s00180-011-0229-5>.
- Hurley, C. and Oldford, R. (2011b), Graphs as navigational infrastructure for high dimensional data spaces, *Computational Statistics*, 26(4), 585–612.
- Jaworski, P., Durante, F., Härdle, W. K., and Rychlik, T., eds. (2010), *Copula Theory and Its Applications*, vol. 198, Lecture Notes in Statistics – Proceedings, Springer.
- Mashal, R. and Zeevi, A. (2002), Beyond Correlation: Extreme Co-movements Between Financial Assets, (2016-04-05).
- McNeil, A. J., Frey, R., and Embrechts, P. (2015), *Quantitative Risk Management: Concepts, Techniques, Tools*, 2nd ed., Princeton University Press.
- Oldford, R. W. (2016), Self-Calibrating Quantile–Quantile Plots, *The American Statistician*, 70(1), 74–90.
- Oldford, R. W. (2014), qqtest: Self calibrating quantile quantile plots for visual testing, R package version 1.1.1.
- Patton, A. J. (2006), Modelling Asymmetric Exchange Rate Dependence, *International Economic Review*, 47(2), 527–556, (2016-06-08).
- Patton, A. J. (2013), Copula Methods for Forecasting Multivariate Time Series, *Handbook of Economic Forecasting*, ed. by G. Elliott and A. Timmermann, vol. 2, Springer, (2016-06-08).
- Rosenblatt, M. (1952), Remarks on a Multivariate Transformation, *The Annals of Mathematical Statistics*, 23(3), 470–472.
- Scarsini, M. (1984), On measures of concordance, *Stochastica*, 8(3), 201–218.
- Schmid, F. and Schmidt, R. (2007), Nonparametric inference on multivariate versions of Blomqvist’s beta and related measures of tail dependence, *Metrika*, 66, 323–354.
- Sklar, A. (1959), Fonctions de répartition à n dimensions et leurs marges, *Publications de L’Institut de Statistique de L’Université de Paris*, 8, 229–231.
- Wilkinson, L., Anand, A., and Grossman, R. L. (2005), Graph-Theoretic Scagnostics. *INFOVIS*, vol. 5, 21–28.